Felix Lichtenegger, Bsc

Ray-tracing based visible light communication channel modelling and its application in a fingerprinting-based visible light positioning system

MASTER'S THESIS

to achieve the university degree of

Master of Science

Master's degree programme:

Physics

submitted to

Graz University of Technology

Supervisor

Assoz. Prof. Dipl.-Ing. Dr.rer.nat., Andreas Hohenau

Institute of Physics

8010 Graz, Universitätsplatz 5

Graz, November 2020

AFFIDAVIT

I declare that I have authored this thesis independently, that I have not used other than the declared sources/resources, and that I have explicitly indicated all material which has been quoted either literally or by content from the sources used. The text document uploaded to TUGRAZonline is identical to the present master's thesis.

Date, Signature

Abstract

Visible Light Communication (VLC) is data communication using electromagnetic waves in the visible spectrum. Data are encoded into light intensity modulations of the light emitted by a luminaire such as a light emitting diode (LED) and are demodulated again after they have been recorded by a receiver device such as a photodiode. The widespread use of LEDs has made VLC an attractive candidate to base positioning systems on. An advantage of a visible light positioning (VLP) system is the use for indoor environments where conventional positioning systems such as GPS are limited. In this work we develop a ray-tracing based channel model which is a powerful tool to determine channel characteristics of VLC settings. In order to overcome the huge computational effort that is necessary in this regard, new strategies for less time-consuming ray-tracing based channel models are essential. We demonstrate that in a virtual test room, several receiver positions can be simulated simultaneously instead of having to run a ray-tracing simulation for each individual receiver position inside the room, because the error made by this approach turns out to be negligible. This channel model is then used for the theoretical conception of a new VLP system based on fingerprinting and angular segmented photoreceivers. The biggest disadvantage of fingerprinting based positioning systems is the time-consuming procedure of having to survey the room in real life regarding the received signal characteristics to obtain the fingerprint-map. We take advantage of the data transmission capabilities of luminaires, assuming they can transmit certain parameters such as their position inside the room to a user's device which in turn uses the information to calculate the fingerprint-map in a simplified manner. We show that with a very simplified estimation for the fingerprint-map the positioning system can theoretically achieve accuracy of several centimeters depending on the system parameters.

Keywords – *Ray-tracing; Visible light communication; Visible light positioning; Channel model; optical simulation*

Table of contents

1. Introduction

Since the first demonstration of the electrical telegraph in the 19th century, the world has evolved to an ever-increasing connected society, more and more dependent on telecommunications. Telecommunications has undeniably contributed to the rapid technical development and industrialization of the world and most areas of our everyday life would be unthinkable without it. The average 21st century person is connected to the World Wide Web via a press of a button at almost any given time by a personal smartphone. Many aspects of private life and also the business world are now happening on the internet. To even make this possible, radio frequency engineers have developed clever ways to cope with increasing band width demand, for example by applying multiplexing schemes in data transmission. However, projections show that mobile data demand will increase exponentially over the next years [1]. Increased worldwide adoption of smartphones is only one of the reasons leading to these projections, but also the emergence of connected devices of everyday life contribute to these figures. Wearable devices such as smart watches, fitness trackers and digital glasses will drive applications in technologies high in data demand, such as high definition video streaming, Virtual Reality (VR) and Augmented Reality (AR)[2] not only for home entertainment but also by adoption in Industry 4.0[3]. Sensor-rich devices, both personal and industrial will drive data demand and bandwidth demand. The ensemble of all devices, communicating with each other (machine to machine communication, M2M) and to the internet, form a new network, the Internet of Things (IoT).

In recent years, visible light communication (VLC) emerged as a technology primed to tackle the problem of increased bandwidth demands of the future [2]. In VLC, data are encoded into light intensity modulations of light emitted by light emitting diodes (LEDs). These modulations can be recorded by a receiver device like a photodiode, where they are demodulated again, and the data is sent to the desired destination. Other forms of Optical Wireless Communication (OWC) like wireless infrared communications (WIRC) and wireless ultraviolet communications (WUVC) have been studied before VLC, however they are like RF systems not license free and have been deployed for military and medical use cases [4]. Furthermore, VLC possesses the ability to provide illumination and wireless data transmission at the same time. The human eye is not able to detect these light intensity variations due to the high pulsation speed of these modulations, as the typical flicker

threshold of the human eye is 3 kHz [5]. The visible spectrum offers the entire unlicensed bandwidth from 430-770 THz which is only subject to eye and skin safety regulations, therefore VLC is primed to be one of the key technologies to tackle the problem of increasing bandwidth demand in the future.

Wireless networking using VLC is referred to as LiFi (light-fidelity) and was first introduced in 2011 by Dr. Harald Haas, one of the leading researchers of VLC technology [6]. In some cases, news titles from popular science media give the impression that LiFi could replace WiFi, which of course is not right [7]. Instead, both systems will coexist and provide mutual relief to the general bandwidth demand. When a user moves out of the coverage area of a LiFi access point, there will be a seamless handover to e.g. Long-Term-Evolution (LTE). This handover between two access points of different systems is categorized as vertical handover [2]. The underlying physical properties of the frequencies of electromagnetic waves alone lead to different application fields. Due to the physical nature of light, the VLC signal can not penetrate through walls, making it a very secure system that cannot be intercepted from the outside. Compared to radio waves, there is no interference with VLC. This feature makes the technology particularly interesting for use in hospitals or aircraft cabins to prevent interference with critical electronic components. Another research group investigated the application of VLC in an underwater environment e.g. for the communication of divers, which is not considered a feasible environment for RF communication [8].

LEDs have penetrated almost all light-emitting devices of our daily lives, including luminaires for general lighting, street lighting or background lighting of displays and has therefore become the most commonly used light source [9]. Adoption of VLC technology can be accelerated by accessing this already existing LED lighting infrastructure with only minimal modifications [10]. VLC benefits greatly from the sought-after properties of LEDs, such as their longevity, robustness against humidity, cool operation, and low energy consumption, resulting in CO2 savings.

From the widespread use of LEDs in interiors, a further application area of VLC has emerged: There is a lack of a reliable, cheap and above all universally applied indoor positioning system. Since the Global Positioning System (GPS) became available to the civilian population, it has been the dominant (outdoor) positioning system globally. GPS requires

line of sight to four satellites, therefore several situations arise where GPS cannot be used, or only with unsatisfactory accuracy. Large buildings, walls, clouds, and other large objects lead to satellite signal attenuation, rendering GPS as an unfeasible indoor positioning system. VLC technology has sparked the interest of the scientific community for its utilization in indoor positioning systems, referred to as visible light positioning (VLP). Many works with varying levels of positioning accuracy, including simulations and real world prototypes have been reported [11,12,13].

Fingerprinting, also referred to as scene-analysis, is a positioning technique where a mobile device determines its position by comparing live signal measurements, to a database that groups signal characteristics (the fingerprint) with their associated location inside the room. The most common characteristic used in fingerprinting positioning systems is the received signal strength (RSS). In this thesis, a novel fingerprinting approach is presented that aims to tackle one of the main disadvantages in VLP fingerprinting:

To construct the reference dataset, a series of measurements, called the offline phase, must first be carried out that collect e.g. RSS information along the corresponding position inside the room. The density in which the sample measurements are performed is an important trade off that determines the probability of accurate localization [14]. The need for the offline phase is one of the main disadvantages in fingerprinting positioning systems, as it is a time consuming and therefore costly process, which must be performed for each unique room separately. While current literature, acknowledges the drawbacks of fingerprinting positioning techniques, there has not been a solution to this problem which would give this technique the required flexibility and ease of installation that is needed for large scale implementation of such a system.

In this work we present a novel fingerprinting-based positioning technique that mitigates the need for the time-consuming offline phase. We take advantage of the VLC data transmission capabilities of the luminaires, to transmit information on lighting configuration inside the room and LED parameters to the user's device, once he enters the room. Based on the transmitted parameters, the mobile device calculates a reference map of directional light intensity distributions in dependence of the location of the room by using a simplified analytical formalism of the illumination pattern of the luminaires and the computational power of a smart phone device. This system requires a receiver capable of discriminating

light impinging on the device from different directions. These types of receivers are referred to as angle diversity receivers (ADR).

In order to identify the optimum parameters, receiver configuration, number of angular segments, the optimum system configuration and to test different approaches a mathematical representation of the simulation environment was created by utilizing the commercial ray-tracing software ASAP. This mathematical model of the communication channel is called a channel model. A proper channel model is a helpful tool in system design, assessment, and optimization. With the help of a channel model it is possible to acquire the channel impulse response (CIR) in a given environment in consideration of reflections and scattering on surfaces in the room. The CIR determines received signal power versus delay time. It is a primary channel characteristic since other characteristics such as time dispersion parameters are calculated from the CIR values.

In this work, I present my work on the theoretical groundwork for such a VLP system based on ADR receivers. The work is structured as follows: Section 2 deals with different methods of channel modeling and contains the self-developed ray-tracing based channel model and advantages thereof. Furthermore, the channel model is applied to a test scenario while presenting a new time-saving simulation technique. In Section 3 the state of the art regarding angular diversity receivers for VLP. Subsequently I will present my personal VLP system based on fingerprinting and angle diversity receivers, which was developed with the ray-tracing based channel model, introduced in Section 2.

2. VLC Channel Modelling

The simplest possible VLC set-up consists of an LED and a photodiode that act as transmitter and receiver, respectively. This setup is depicted in Figure 1. The data are encoded and modulated by applying different modulation techniques. The modulated output power of the LED emission is received by a photodiode which is located at an arbitrary position in the room, where the signal is demodulated again.

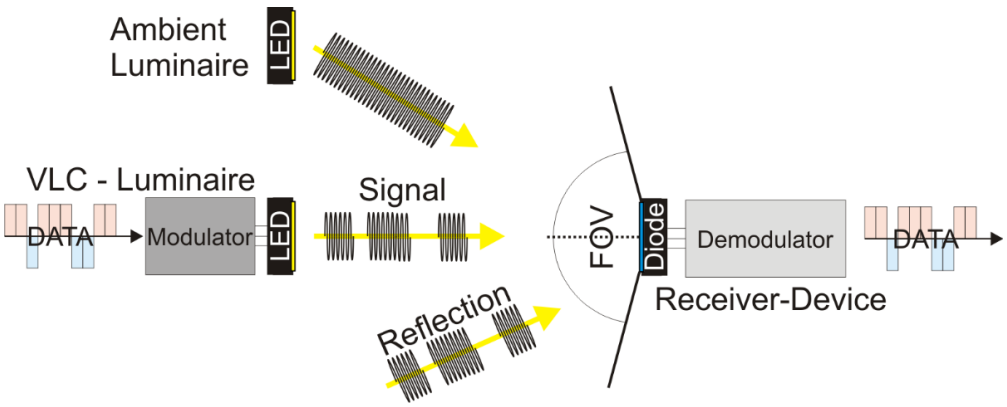

Figure 1 Sketch of the basic set-up of a VLC setting consisting of a luminaire emitting intensity modulated light and a receiving device recording this intensity modulation. The signal to noise ratio of the recorded intensity modulation is strongly affected by (varying) ambient and daylight contributions and reflection events of the intensity modulated light.

However, there are many potential sources for a deterioration of the modulated signal before it reaches the photodetector. This includes, e.g., the interaction of modulated light from one luminaire with light form other luminaires or with daylight as well as specular and diffuse reflections of the modulated light by the room environment (walls, furniture…) or shadowing effects, e.g., by inhabitants. This strongly affects the signal to noise ratios, in particular with respect to the location of the receiver device in the room.

In order to identify strategies to improve these signals to noise ratios for a VLC set-up inside a room, the use of a mathematical representation of the communication channel, a so-called channel model, is a promising approach. A proper channel model is a helpful tool in system design, assessment, and optimization. With the help of a channel model it is possible to acquire the channel impulse response (CIR) in a given environment. The CIR determines received signal power versus delay time. It is a primary channel characteristic since other

characteristics such as time dispersion parameters are calculated from the CIR values. Several simulation strategies have been followed in this regard.

2.1 Existing Channel Models

A multitude of channel models for Optical Wireless Communication (OWC), e.g. wireless infrared communications (WIRC), have been published in the past. IR channel models have been deployed for estimating CIR in VLC systems [15,16], however, to properly model a VLC channel, one has to take into account the differences between WIRC and VLC systems. In IR systems, the IR source can be modelled as monochromatic, while in VLC systems the source, e.g. a white LED, emits power over a broad spectrum of wavelengths (380-780nm), which cannot be neglected. Another point to consider is the reflectivity of materials. Reflectivity values are (near-) constant in the IR spectrum, but in the visible spectrum reflectivity values strongly depend on the wavelength. Considering the usage of VLC for data communication and illumination, a proper channel model should take into account the physical dimensions, radiation pattern and spectral power distribution of commercial LEDs.

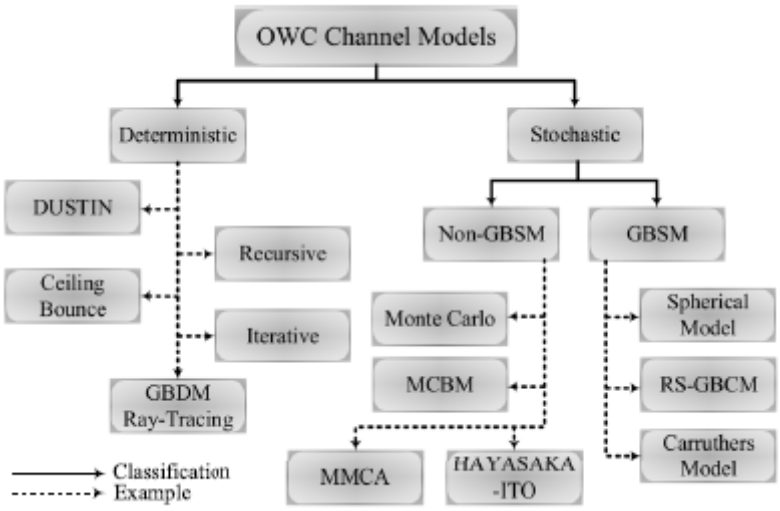

Figure 2 Classification of Optical Wireless Communication (OWC) channel models, adopted from Al-Kinani et. al. [5]

Channel Models from previous works can be grouped into certain categories. One way of categorization for optical wireless communication channel models is presented by Al-Kinani et. Al.[5], depicted in Figure 2. The authors categorize efforts for channel modelling, including channel models for other forms of OWC besides VLC such as WIRC. The first distinction they make, is between deterministic models and stochastic models. Deterministic

models rely on the detailed description of the channel environment, like room dimension, position and orientation of sender and receiver and description of reflections. Therefore, deterministic channels are site specific and the channel impulse response for a specific environment is determined by complex simulations. Stochastic models on the other hand, offer a non-site-specific description of the communication channel with more flexibility but also lower accuracy. The channel impulse response is attained by the law of wave propagation and specific scattering behavior, applied to a probability distribution.

Stochastic models are further grouped into geometry based deterministic models (GBDM) and non-geometry base deterministic models (NGBDM).

Ramirez-Aguilera et. Al. use three groups of channel models to characterize existing indoor optical wireless communication channel models [17]: Analytical, iterative (or recursive), and stochastic. The authors justifiably argue that it is important to understand the historical development of OWC channel models, in order to grasp the state-of-the-art in VLC channel modelling, as many of the channel modelling techniques for OWC (mostly WIRC) have been extended to be applied in VLC channel modelling. The following paragraph will give a short summary of significant works, in OWC channel modelling which will serve as the bridge to my own efforts regarding channel modelling in VLC.

The first efforts to analytically model the received optical power in an OWC were published by Gfeller and Bapst in 1979 [18]. They proposed to use diffuse optical radiation from LEDs in the near infrared as a signal carrier in an indoor environment. Through analytical description and experimental verification, they explored the potential and limitations of such an optical channel. The study was limited to one reflection only, due to the exponential increase in computational effort when considering more than one reflection. As an alternative, Barry et. Al. published their recursive channel model, which is capable of handling any number of reflections, limited by only simulation time effort [19]. The model is based on the division of surfaces into small cells which are characterized by their reflection coefficient and their area, assuming only diffuse reflections. In their paper, they showed that the multipath dispersion is a significant source for intersymbol interference. Many works have been published based on Barry's model, contributing improvements to the method. The main drawbacks of these models are the relatively high computational cost and the assumption of only diffuse

reflectors, which is not given in real life scenarios [9]. By combining ray tracing with Monte Carlo numerical techniques, Loped-Hernandez et. Al. introduced a new type of iterative model to calculate the impulse response in indoor optical infrared channels [20]. The algorithm is capable of modelling Lambertian scatter and also specular reflections. The main reason for long simulation times is the high number of rays that have to be generated at the source. The low probability of a ray hitting a receiver comes from the difference in size dimensions of the whole simulation environment compared to the small size of the receiver. To combat this, the same authors introduced the Modified Monte Carlo Scheme (MMC) which greatly reduces the necessary number of rays that have to be generated [21]. This is achieved by assuming a contribution to the receiver for every ray and also for every reflection of a ray. MMC has been adopted by other groups that have published their works. For example, Chowdhury et. Al. combined MMC with a deterministic approach [22]. For the contributions of the first reflections they used a deterministic approach, while second and higher order contributions to the impulse response are calculated via MMC. In [23] Ramirez-Aguilera et. Al. introduced the multi-wavelength Matrix-MMC model with the capability of capability of capturing reflection phenomena implying changes on wavelength (eg. fluorescence, phosphorescence, or iridescence). For statistical models it is first necessary to collect data from either experiment, simulation, or both. For example, Perez-Jimenez et. Al. proposed a statistical model for calculating impulse response in a WIRC [24]. Estimates for time dispersion parameters are based on coefficients in an analytical expression. The shape of the channel impulse response is fitted by Rayleigh distributions or Gamma distributions. Finally the total received power is calculated by the well-known power budget approximation [25].

The first channel model for VLC based on non-sequential ray tracing was presented by Sarbazi et. Al. [26] and Miramirkhani and Uysal [27]. The model is developed in the commercial optics and design software Zemax®. This channel model based on non-sequential ray tracing has been motivated by the limitations of other channel models in the visible spectrum. As mentioned above, many VLC channel models are based on the earlier channel models developed for the IR spectrum. In IR systems, the IR source can be modelled

as monochromatic, while in VLC systems the source, e.g. a white LED, emits power over a broad spectrum of wavelengths (380-780nm), which cannot be neglected. Another point to consider is the reflectivity of materials. Reflectivity values are (near-) constant in the IR spectrum, but in the visible spectrum reflectivity values strongly depend on the wavelength. In [28] a recursive model is used for VLC channel model, but only assuming constant reflectivity values over wavelength. Another simplification approach is used in [29] where an average reflectivity value is calculated for all wavelengths. The methodology of calculating CIRs in indoor settings presented by Miramirkhani et. Al. offers great flexibility and is capable of overcoming the limitations of other models mentioned above. The methodology served as inspiration for my own channel model, with the difference being that Miramirkhani et. Al. chose Zemax as the ray tracing platform and we chose ASAP. The following chapter on non-sequential ray tracing-based channel modelling is structured in an short introduction on non-sequential ray tracing, methodology of the channel model, verification of the channel model and finally demonstrations of capabilities and advantages of this model.

2.2 Non-sequential Ray Tracing

The channel model is based on optical simulations using non-sequential ray-tracing in combination with self-developed algorithms in MATLAB. For the ray-tracing part, the commercial software ASAP (Breault Research Organization) is used.

In non-sequential ray tracing the order in which objects are hit by a ray only depend on the individual ray that is being traced. There is no pre-defined sequence of objects that must be hit. Rays are traced through the simulation environment by the laws of geometric optics. Geometric optics is an approximation for describing the propagation of light. In this model light is described as a straight ray while wave phenomena such as coherence of the electromagnetic wave are neglected. In the overlapping area of ray bundles interference can occur but after the bundles are spatially separated their intensity distribution is again as if the other bundles were not present [30]. This approximation is permissible in a system where the wavelength is much smaller than the dimensions of the relevant objects in the system. The propagation of beams can be summarized in three basic axioms:

1) In optically homogeneous media, light rays are straight.

2) At the boundary of two isotropic media, light rays are generally refracted by the law of refraction and reflected by the law of reflection.

3) Rays can be superimposed, but do not influence each other any further.

ASAP is capable of modeling the optical characteristics of the indoor environment considering the reflection properties of the walls and objects in the room. Light sources are defined by means of their positions in the room, their radiation patterns, their spectral power distributions and their total emitted powers. All physical objects are modelled as geometrical surfaces. It is necessary to define a reflectivity value for each of these surfaces or, alternatively, to use scatter models implemented in ASAP. Scatter models are characterized by their Bidirectional Scatter Distribution Function (BSDF), which is defined as the ratio of differential radiance from a surface and the differential irradiance the surface is illuminated by. It describes the angular distribution of radiation scattered from a surface. The simplest scattering model in ASAP is the Lambertian scatter model, where the scattered light shows no dependence on angle of incidence. Therefore, the Lambertian BDSF is a constant.

This method also supports the implementation of CAD models, e.g., of room furniture like it was demonstrated in [27] Thereby a realistic and accurate model of a room is created. Also, the optical characteristics of the luminaire and the receiver device can be taken into consideration with this method.

2.3 Methodology of the channel model simulations

For the ray-tracing simulations it is necessary to define the simulation setting with all relevant optical parameters and characteristics. ASAP creates a user defined number of rays at the light sources and traces their paths through the simulation setting. In dependence of the chosen surface characteristics, a ray can be either scattered or specular reflected. ASAP offers different models for describing the scattering of rays. These models vary in complexity and therefore in computational time. A Lambertian scattering function has the advantage of relatively low computational times when compared to other models, and also allows considering the diffuse scattering characteristics of some materials surfaces like a white plaster of a room wall. Lambert's cosine law of reflection determines the scattering direction of a ray by a probabilistic process.

For a light detecting unit fully absorbing surfaces are deployed in the simulation setting. When a ray hits such a receiver unit, the ray is stopped and is no more traced further on. Rays that do not reach a receiver unit before, are either stopped after reaching a user defined, fixed number of allowed reflections k, or by setting a minimum threshold for the flux that is carried by a ray. As pointed out by Miramirkhani et al. in [27], channel modeling based on ray-tracing is capable of handling any number of reflections and therefore offers more flexibility than other channel modeling approaches, such as an analytical approach. In the related study, the authors showed that there is no noticeable change in channel characteristics, e.g., received power or time dispersion parameters, for a maximum number of reflections k=4 or larger within the investigated scenario. In order to save computational time the number of allowed reflections for each ray is fixed to a maximum of k=3 in the present study. The characteristics of the rays, that reach a receiver surface, are logged into a text file containing all relevant information about these rays, such as location, direction, flux, optical path length, number of object intersections and wavelength.

Table 1 Ray information in ASAP that can be stored in the output file, which is forwarded to Matlab for calculation of channel characteristics and further analysis.

Register	Literal	Ray/Beam Data
A0, B0, C0	**X,Y,Z_DIR_B**	**Absolute XYZ direction cosines**
Ai, Bi, Ci	X,Y,Z_DIR_i	Relative direction vector of ith parabasal ray
D0	**OPL**	**Optical path length from start of base ray**
E1, E2, E3	X, Y, Z_EPOL	Components of unit polarization vector
F0	**FLUX**	**Total flux in ray**
G0	DIVERG	Average divergence angle of beam
H0	HEIGHT	Average height of beam centered on base ray
Ii	PREV_O_i	Ith previous split object for ray/beam
J0	**SOURCE**	**Source number from which ray/beam originated**
K0	**CURR_OBJ**	**Current object at which ray/beam is located**
L0	**HITS**	**Total number of surfaces ray has hit (intersected)**
M0	MEDIUM	Medium that ray/beam is in
N0	SPLITS	Number of times ray/beam has been split
N1	**LEVELS**	**Number of times ray/beam has been scattered**
P0	POLAR_0	Relative modulus of fundamental beam mode
P1, P2	POLAR_1,2	Relative moduli of polarization components
Q0	**NUM_RAYS**	**Total number of ray/beams**
Q1	NSOURCES	Total number of original sources
R0	PARENT	Number of ray from which this ray was split
S0	SHAPE	Beam shape factor or number (SHAPE command)
S1	FACTOR	Beam shape factor or number of higher modes
T0	PHASE_0	Relative phase angles of fundamental beam mode
T1, T2	PHASE_1,2	Relative phase angles of polarization components
U0, V0	U, VPARAMB	Parametic coordinates of base ray position
W0	**WAVELEN**	**Wavelength of ray/beam**
Wi	WAVLNS_i	Wavelength for ith source
X0, Y0, Z0	X, Y, Z_POS_B	Global X, Y, Z coordinates of base ray
Xi, Yi, Zi	**X, Y, Z_POS_i**	**Relative coordinates of ith parabasal ray**

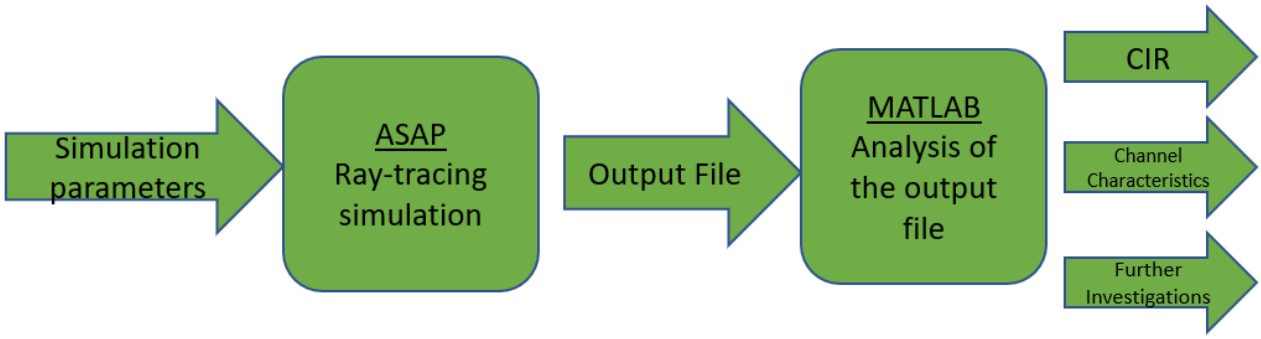

Figure 3 Methodology of non-sequential raytracing-based channel modelling. From the ASAP simulation an output file containing information on each ray that hit a light detecting unit is stored. This file is forwarded to Matlab, where the channel impulse response is calculated with the data provided in the output file. Further investigations are possible.

Table 1 lists all ray properties that can be exported from asap via the output file. The information from this table that is used for this channel model study is marked in bold font. This list of ray characteristics is forwarded to MATLAB for further analysis. This process of the simulation methodology is shown in Figure 3. The CIR values can be calculated from the information provided by the imported ray file, especially from the optical path length of the rays, which can be used to calculate the time of arrival of each ray on the receiver surface. Other channel characteristics subsequently can be calculated from the CIR values. For instance, the channel DC gain is a further key characteristic of the channel as it measures received power. Therefore, it is a measure of the achievable signal-to-noise-ratio and the maximum achievable bit rate [5]. For the characterization of time dispersion, two time dispersion parameters are usually used: the mean excess delay and the root mean square delay.

2.4 Channel Characteristics

In what follows, a mathematical description of the most commonly used channel characteristics is given. The **Channel Impulse Response** h(t) can be expressed by

$$h(t) = h^0(t) + \sum_{k=1}^{\infty} h^k(t)$$

where h^0 is the line-of-sight- or direct- component of the signal and h^k represents components that have undergone k reflections. It measures the power over time delay of the received signal. To calculate CIR in non-sequential raytracing a more convenient form of the CIR can be used:

$$h(t) = \sum_{i=1}^{N} P_i \, \delta(t - \tau_i)$$

In this form of the CIR, N is the total number of rays, P_i is the power of the ith ray and τ_i is the propagation time of the ith ray. To assign each ray to the correct time slot the Dirac Delta function δ is used.

As mentioned earlier the CIR is the primary channel characteristic as it is the starting point to estimate other channel characteristics in the given simulation scenario. It is the time evolution of a infinitesimal short signal received by the receiver unit. Therefore, with the CIR one can obtain the profile of the received signal from that of the transmitted signal.

The **Channel DC Gain** H_0 is calculated by integration of the CIR

$$H_0 = \int_{-\infty}^{\infty} h(t)dt$$

and is interpreted as the fraction of power detected at the receiving unit. Depending on the scenario, in regards to modulation technique applied to the signal, the signal-to-noise ratio is proportional to channel DC gain, as it measures the received power at the receiver unit.

Another main aspect in channel modeling is time dispersion of signals. Due to reflections in the channel environment, the signal appears as a sum of delayed copies of the signal in the form of line-of-sight and non-line-of-sight components. From the difference in path length, signals take through the environment comes the time dispersion. The most commonly used metrics for time dispersion are the **mean delay spread** τ_0 and **the root mean square delay spread** τ_{RMS}.

$$\tau_0 = \frac{\int_0^{\infty} t \, h(t)dt}{\int_0^{\infty} h(t)dt}$$

$$\tau_{RMS} = \sqrt{\frac{\int_0^{\infty} (t - \tau_0)^2 \, h(t)dt}{\int_0^{\infty} h(t)dt}}$$

Small values indicate low dispersion and result in a higher bit rate. The **maximum achievable bit rate** B in a given system is dictated by the root mean square delay spread in the form

$$B = \frac{1}{10\,\tau_{RMS}}$$

-

2.5 Verification of the Channel Model

In order to verify the accuracy of the channel modeling approach introduced in this study, the related results are compared with those of Miramirkhani et al. in [27], in which the authors used the commercial optical and illumination design software Zemax for ray-tracing based channel modeling. In accordance with their study, the simulated room has dimensions of 5 m x 5 m x 3 m with four luminaires L1-L4 on the ceiling, each consisting of 100 LED chips and a 1 cm^2 receiver located on the floor of the room as seen in figure 4.

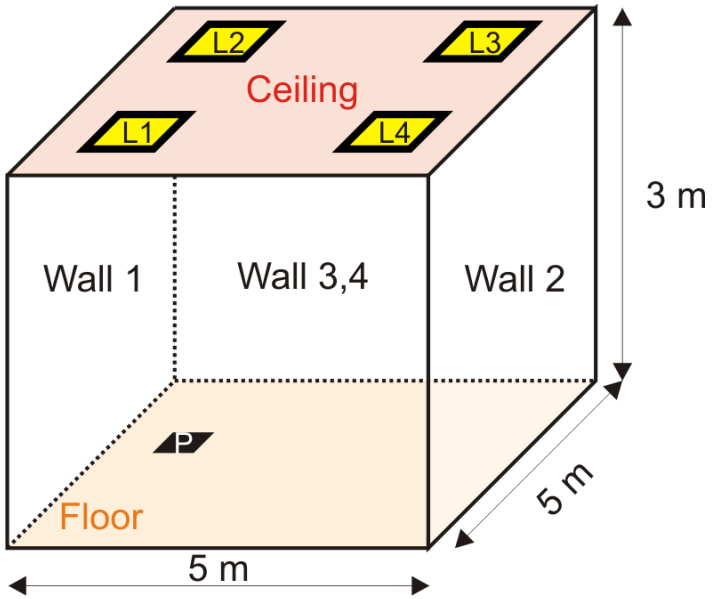

Figure 4 Simulation setting *for verification of the channel modeling method introduced in this study. The 5 m x 5 m x 3 m room contains 4 luminaires, consisting of 100 LED dice each, and one receiver unit (photodiode, P) located on the floor of the* room. The simulation setting is in accordance with that reported in [21].

Each LED die emits with a radiant power of 0.45 W and has a Lambertian radiation characteristic confined to a cone angle of 120°. While Miramirkhani et al. used a realistic

model of a commercially available LED die (Cree Xlamp MC-E White LED), we modelled the LED dice as square-shaped, light-emitting surfaces, which were modified in their radiation characteristics to meet all the desired parameters listed in Table 2, in accordance with the simulation settings of [27]. The spectral power distribution of the LED emission was also taken over from [27] and was modelled with 13 sample points. For each of the related wavelengths, we ascribed relative radiant powers in accordance with those reported for the Cree Xlamp MC-E LEDs and reflectivity values for ceiling, floor and white plaster of the walls (Figure 5) in accordance with the values reported in [27].

Table 2 Parameters of the simulation setting

Size of room	5[m] x 5[m] x 3[m]
Time Resolution	0.2 [ns]
Number of luminaires	4
Number of LED dice per luminaire	100
Number of rays for each die	400000
Radiant power of each die	0.45 [W]
Luminaire positions	(1.5,1.5,3) [m] (1.5,3,3) [m] (3.5,1.5,3) [m] (3.5, 3.5,3) [m]
Receiver position	(0.5,1,0) [m]
Cone angle of LED emission	120°
Field of view of receiver	85°
Area of receiver	1 [cm^2]
Scattering model	Lambertian Scattering

The reflectivity values are based on the spectral reflectance measurements provided in [27]. The size of the receiver is comparatively tiny to the size of the room, which means that a very high number of rays have to be used in this simulations. To ensure a sufficient number of rays (> 8000) hitting the receiver surface during the ray-tracing simulation 400k rays were used for the simulation of every LED die resulting in a total number of 160 million rays for the whole simulation. Such a large number of rays strongly increase the simulation time of a ray-tracing simulation. A whole simulation sweep with 13 different wavelengths takes about 12 hours of simulation time with a standard workstation.

Figure 6 shows the resulting channel impulse response for the simulation setting depicted in Figure 4, when using the channel modeling technique introduced in this study and the relative radiant power values of Figure 5 a) and the spectral reflectivity values for the ceiling, the floor and the white plaster of the walls as shown in Figure 5 b). Except for the absolute power values of the CIR, the result is in good accordance with the results of Miramirkhani et al. in [27], which in conclusion shows, that the suggested simulation method allows for credible results. The difference of the absolute power values can be explained by the fact that the optical model and therefore the totally integrated emitted power of the LED dice may slightly differ from the model used in [27].

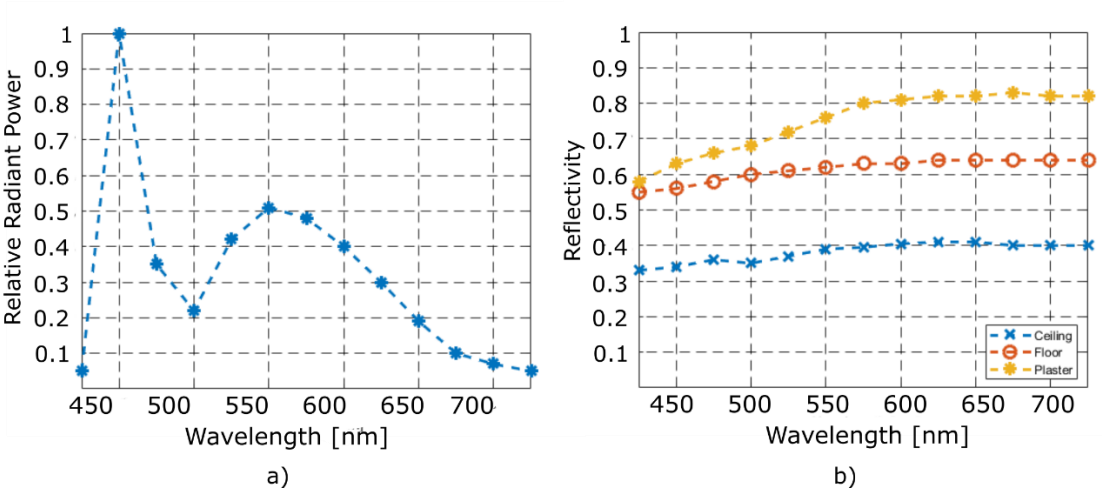

Figure 5 a) Relative radiant power of the modelled LED surfaces in the simulation. b) Reflectivity values for ceiling, floor and the plaster of white walls.

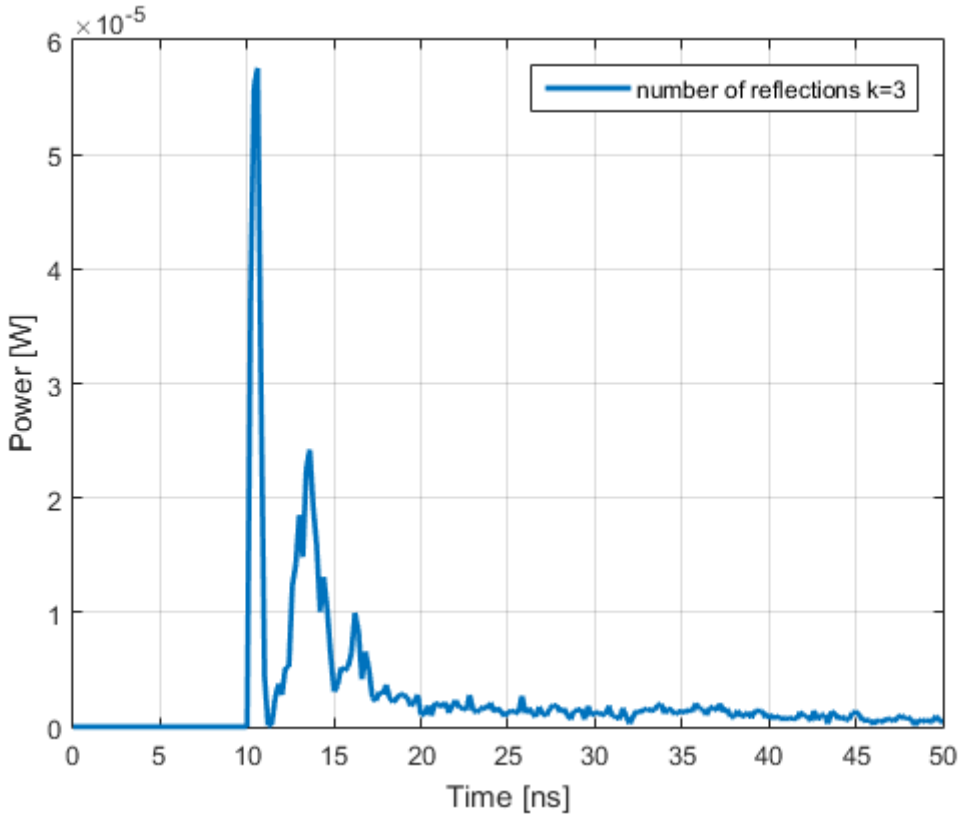

Figure 6 Channel Impulse Response as determined for the simulation setting with a maximum number of allowed reflections of k=3.

2.6 Applications of the channel model

2.6.1 Simultaneous simulation of variable receiver positions along a defined path

One application of the proposed channel model based on optical design software is to investigate the influence of different reflectivity properties of surfaces inside the room on the VLC channel characteristics in dependence of the receiver position. With the help of this, one can identify surface characteristics and receiver positions which allow for optimized channel characteristics. For such a study many receiver positions inside the room have to be simulated in individual simulation runs to determine the position dependence of the VLC parameters. In the following application example, we show a simulation approach to largely reduce the number of simulations needed in this regard. Figure 7 shows the simulation setting to demonstrate the capability of the developed channel model: The reference simulation setting is again representing a 5 m x 5 m x 3 m sized room composed of different surfaces representing

the ceiling, the floor and 4 walls which have the same Lambertian scattering properties as already defined in section 2. On the ceiling, again 4 luminaires are placed, each composed of 10 x 10 emitting surfaces, representing the emitting surfaces of LED dice, each of them with a Lambertian radiation characteristic confined to a cone angle of 120°.

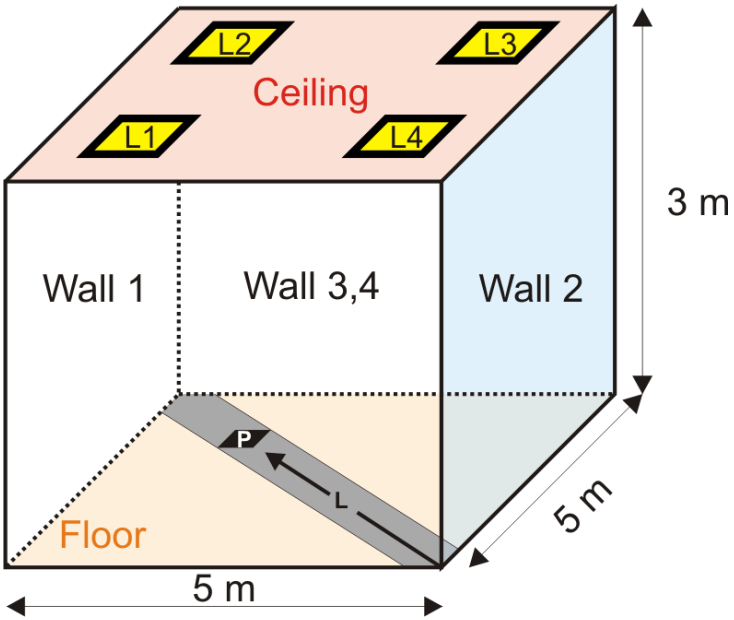

Figure 7 Schematic of the investigated simulation setting of a room with 4 luminaires on the ceiling (L1-L4). Wall 3 is defined to be in front, wall 4 is defined to be in the back of the setting. The position of the VLC receiver can be varied along a diagonal stripe located on the floor of the room, enabling different measurement positions of the VLC receiver along this stripe.

For the simulation of every LED emitting surface 400k rays with a radiated power of 0.45 W were used resulting in 160 million rays per wavelength and an emitted power of 180 W in total for the whole simulation. The number of allowed reflections k of the rays during the ray-tracing simulation is again restricted to 3. The reflectivity values of the walls, the floor and the ceiling and the emitted radiant power of the LED dice are wavelength dependent, therefore 13 independent simulations at different wavelengths ranging from 425 nm to 725 nm in 25 nm steps and using the corresponding reflectivity and emitted radiant power values are necessary for every channel simulation (see Figure 5).

A stripe with a width of ~1.41 cm reaching from the corner enclosing the walls 2 and 3 towards the corner enclosing the walls 1 and 4 (see Figure 7) is placed on the floor and is used as a receiver in this simulation. When rays are hitting the receiver surface all relevant ray data (positions, directions, fluxes, wavelength and optical path lengths) are recorded and exported.

These data are subsequentially evaluated in MATLAB to calculate the VLC channel characteristics. By doing so, many investigations can be done ex post and do not require a new, time-consuming ray-tracing simulation,. For example, one can study the effects of widening or narrowing the FOV of the VLC receiver on the VLC channel characteristics by an ex post selection of incident rays based on their propagation directions. Using a stripe instead of a 1 cm x 1 cm area representing a single photodiode as receiver in the simulation offers a similar advantage. By subsequent selection of incident rays based on their position during the MATLAB evaluation, the position of an, e.g., 1 cm x 1 cm sized receiver can be artificially moved along the stripe, enabling the evaluation of different positions of the receiver with only one ray-tracing simulation sweep of the 13 different wavelengths.

By using such a stripe, an artificial simulation error on the simulation results can be expected because rays that hit the stripe at a non-receiver position during the simulation could be reflected by the otherwise floor surface and then could hit the actual position of the receiver via another reflection. To estimate this error, the influence of the whole floor on the simulation results was determined by conducting a simulation comparing the reference simulation with a simulation setting in which the whole floor was considered to be an absorbing surface. The simulation results indicate a mean deviation of ~4% for the channel DC gain values and ~30% for the RMS delay spread (τ_{RMS}) values, indicating a non-negligible influence of the floor on the VLC channel characteristic values. When the floor is illuminated sufficiently homogeneously, which is the case for the investigated setting, one can assume that the number of rays impinging on parts of the floor directly correlates with the area of the respective parts of the floor. Since the strip has a very small size (diameter of ~1.41 cm), the resulting area is ~0.01 m² which is small compared with the surface of the whole floor of the room (25 m²), and results in a ratio of 0.0004 between the area of the strip and the area of the floor. Multiplying this ratio with the deviations caused by an absorbing floor leads to negligible small values for the artificial simulation errors caused by this procedure.

For investigating the influence of different reflectivity properties of surfaces inside the room on the VLC channel characteristics, the reflectivity properties of wall 2 were varied. Three simulations were conducted in which wall 2 was assumed to have reflectivity values of 100%, 50% and 0%, respectively. The latter case of 0% reflectivity means that wall 2 is fully absorbing. The scattering properties of the wall in addition have been defined to be specular, what

corresponds to reflective surfaces such as mirrors or a very black color in case of the fully absorbing surface.

Figure 8 shows a plot of the channel DC gain in dependence of the distance L of the receiver from the corner enclosing the walls 2 and 3 for the three different reflectivity values of wall 2. The data are given for 26 different receiver positions along the stripe and were determined by the ex post MATLAB evaluations of one ray-tracing simulation run. The channel DC gain value can be calculated by integrating the CIR over time and is directly corresponding to the intensity hitting the 1 cm x 1 cm surface of a receiver at its evaluated position along the stripe. As one can conclude from the results, an absorbing property of the wall is decreasing the intensity hitting the receiver for lower distances (L = 0 – 4 m) from the corner enclosing walls 2 and 3 (and therefore also from the absorbing wall) but has a small impact on the intensity values for receiver positions further away (L = 4 – 7.07m) compared to the reference case for which all walls have Lambertian scattering properties. A mirror like wall (100% specular reflectivity) on the other hand has the opposite effect and is increasing the intensity for receiver positions closer to the corner enclosing walls 2 and 3 (and therefore also from the specular reflecting wall) compared to the reference case and will therefore enhance the achievable signal-to-noise ratio for closer receiver positions.

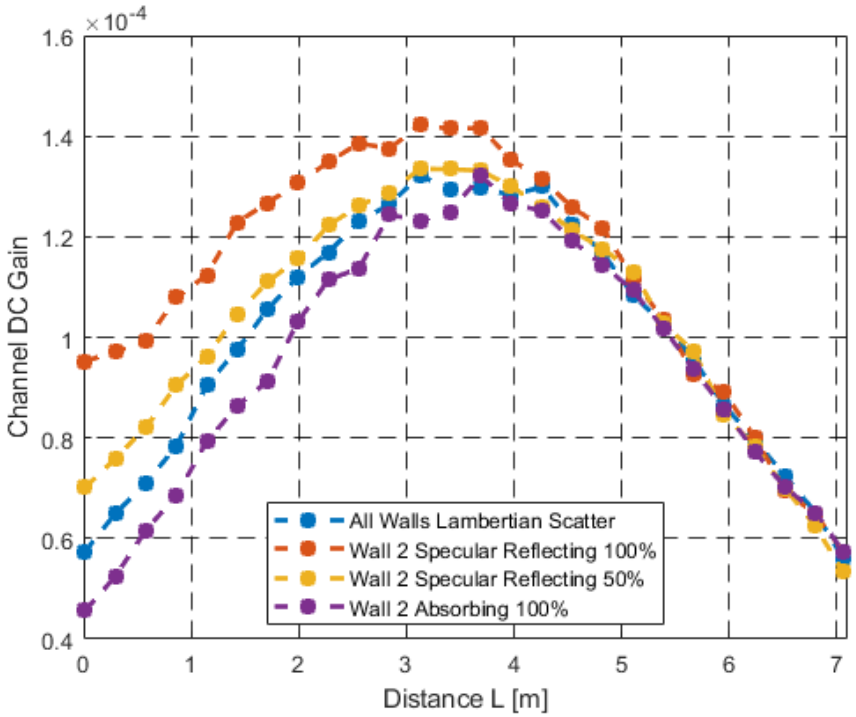

Figure 8 Cannel DC gain plotted in dependence of the distance L of the receiver from the corner enclosing the walls 2 and 3 for three different reflectivity values of wall 2.

Figure 9 shows a plot of the RMS delay spread (τ_{RMS}) in dependence of the distance L of the receiver from the corner enclosing walls 2 and 3 for the different reflectivity values of wall 2. The τ_{RMS} value is an important parameter of VLC because it is restricting the maximal achievable bit rate for data transmission with VLC, for which a low value of τ_{RMS} is indicating a higher achievable bit rate [27].

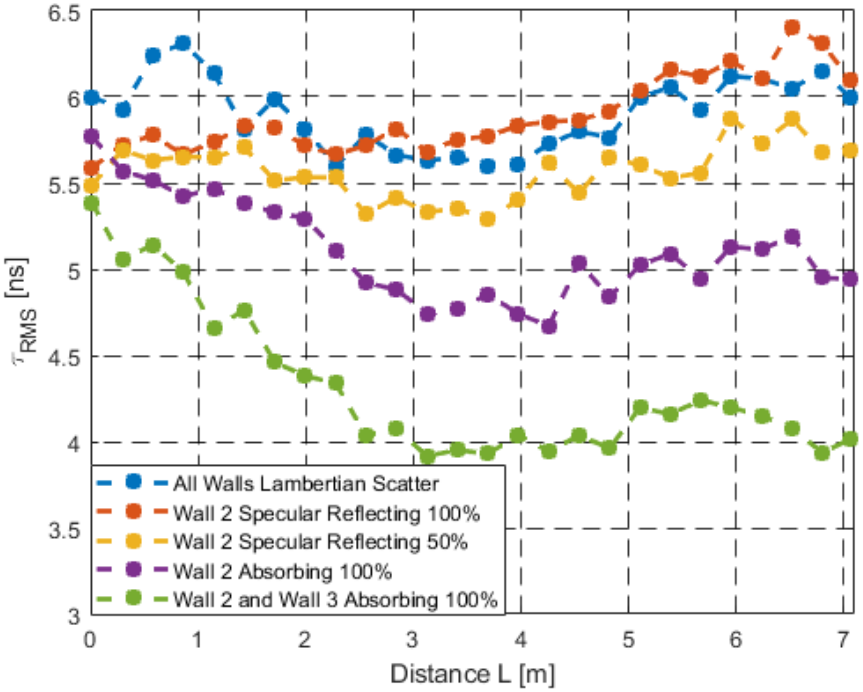

Figure 9 RMS delay spread (τRMS) plotted in dependence of the distance L of the receiver from the corner enclosing walls 2 and 3 for the different reflectivity values of wall 2.

As already mentioned, the τ_{RMS} value is a parameter for the characterization of the time dispersion of the CIR signal. It depends on the strength and the time of arrival of the reflected signals compared to the direct signals and becomes smaller when the reflections are mitigated [31]. As one can see from the simulation results depicted in Figure 9, the τ_{RMS} for the simulation setting with an absorbing wall 2 is satisfying this by showing generally lower values as the reference case, for which all walls have Lambertian scattering properties. Still, for the reference case one would expect a more symmetrical characteristic. However, these simulations suffer from some inaccuracies. Despite the overall large number of rays (160 million), due to the large size of the experimental setting only a small number of rays impinge on a small area within this setting, as it is for example given for a receiver unit. A very interesting result are the comparatively high τ_{RMS} values for receiver positions (L = 0 – 2m) closer to the absorbing wall 2. This can be explained by the fact that not only the strength of the reflected signals have an impact on the τ_{RMS} value but also the time of arrival. Light rays which are reflected from the opposite walls towards the receiver show higher time dispersion than rays reflected from an adjoining wall. Therefore, an opposite wall gives reason for smaller τ_{RMS} than an adjoining wall in case that the reflectivity of the wall is

reduced. To highlight this, another simulation was conducted for which both walls 2 and wall 3 were considered to have absorbing properties. As one can conclude from the simulation results in Figure 9, the observed effect is amplified, especially for higher distances L from the corner enclosing the absorbing walls.

2.6.2 Further capabilities of the channel modeling method

Ray-tracing based channel modeling is a powerful tool for the determination of the channel characteristics of VLC settings. In the previous chapter we introduced an approach, which allows the determination of the dependence of the receiver position on the VLC characteristics along the diagonal of the floor of a room. 26 different receiver positions along the diagonal axis of a room were investigated using only one wavelength dependent simulation sweep instead of 26 independent simulation sweeps for achieving similar results when considering just one single position of the receiver unit. The underlying concept, which makes these investigations possible, is the channel modelling approach based on non-sequential ray tracing, depicted in figure 3. By exporting a file containing relevant information on each ray as determined by ray-tracing, it is possible to do further analysis of the investigated setting without the need for additional ray-tracing simulation runs. A complete list of these ray characteristics is depicted in Table 1. Investigations can be performed ex post and do not require additional time-consuming ray-tracing simulation runs. Examples of ex post investigations include:

- Investigate direct or indirect light only
- Isolation of rays according to the number of reflections
- Switching light sources on and off
- Changing the photodiodes FOV
- Filtering wavelengths

One capability of this channel modeling method is of special interest in the following chapter, where we need to consider the direction of incident light. Figure 10 is an exemplatory visualization of the relative light intensity distribution at room position x=2m and y=3m. The polar angle θ is divided into 3 angular intervals. The azimuthal angle is

divided in 4, 8 and 12 angular intervals from left to right, thereby visualizing the angle of incidence of light from the whole room in one distinct room position.

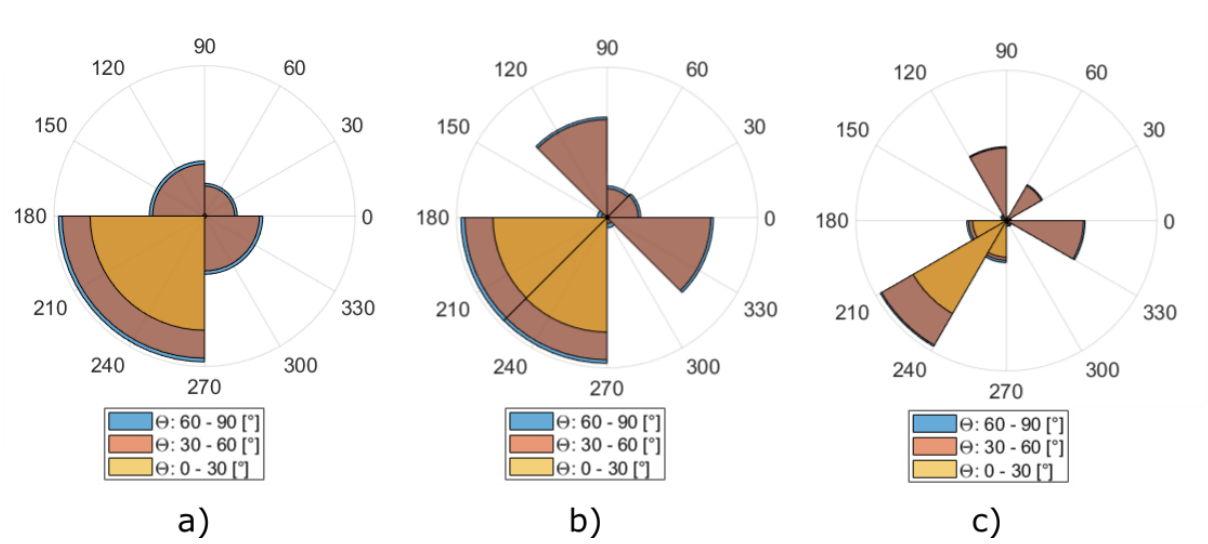

Figure 10 Visualization of the relative light intensity distribution over the azimuthal angle for receiver at position x=2m and y=3m in the room. a) intensity distribution for 4 azimuthal- and 3 polar segments b) intensity distribution for 8 - and 3 polar segments c) intensity distribution for 12 azimuthal- and 3 polar segments.

These investigations can be conducted with relative ease, since the output file containing all the information on all the detected rays is easily manipulatable in Matlab or any other numerical computing environment. Rays in this output file are ignored if they fulfill a certain condiation e.g. the wavelength or the light source they originate from.

3. Visible Light Positioning

In this section of my work, I will take use of the ray tracing based channel model to investigate the feasibility of a new kind of visible light positioning (VLP) system. The VLP system presented here is based on fingerprinting (also called scene-analysis) and the deployment of angular segmented receivers.

GPS has been the dominant positioning system, since it became available to the public. GPS requires line of sight to four satellites, therefore several situations arise where GPS cannot be used, or only with unsatisfactory accuracy. Large buildings, walls, clouds and other large objects lead to satellite signal attenuation, rendering GPS as an unfeasible indoor positioning system [32]. To circumvent this, several radio frequency (RF) based indoor positioning systems were developed, which however suffer from multipath effects and interference. Other approaches, like a LIDAR (light detection and ranging) based systems and camera based scene analysis offer higher accuracy then RF based systems but are costly and require high computational power [33, 34, 35, 36]. Camera-based systems suffer from the very low data rate, which has been identified as the key limitation of this approach [36]. In contrast to that photodiode (PD) receivers can handle very fast data rates, this is the reason why focus on this receiver type in our contribution.

3.1 A short review on existing VLP systems

VLC technology has sparked the interest of the scientific community for its utilization in indoor positioning systems, referred to as visible light positioning (VLP). Many works with varying levels of positioning accuracy, including simulations and real world prototypes have been reported [11,12,13]. VLP systems can be grouped into three categories: proximity, fingerprinting and geometry-based techniques. The relatively simple proximity technique is based on LED base stations that can transmit their identification code to a mobile device, which in turn looks up the identification code with its associated location in a database [11]. In geometry-based techniques, the concept of signal triangulation or trilateration is used to calculate the position of an object relative to the light sources [33]. Different signal characteristics are applicable for determination of distance from light sources. They include received signal strength (RSS), angle of arrival (AOA), time of arrival (TOA) and time

difference of arrival (TDOA). Fingerprinting, also referred to as scene-analysis, is a positioning technique where a mobile device determines its position by comparing live signal measurements, to a database that groups signal characteristics (the fingerprint) with their associated location inside the room.

Fingerprinting, also called scene-analysis is an approach widely used in VLP system [11, 12, 13]. The most common characteristic used in fingerprinting positioning systems is the received signal strength (RSS). To construct the reference dataset, a series of measurements, called the offline phase, must first be carried out that collect RSS information along the corresponding position inside the room. The density in which the sample measurements are performed is an important trade off that determines the probability of accurate localization [14]. The need for the offline phase is one of the main disadvantages in fingerprinting positioning systems, as it is a time consuming and therefore costly process, which must be performed for each unique room separately. Furthermore, if the room changes, e.g. the outage of one luminaire, the reference data set is no longer applicable for fingerprinting as the room configuration in the real world and the room configuration of the collected data set have changed. While current literature, acknowledges the drawbacks of fingerprinting positioning techniques, there has not been a solution to this problem which would give this technique the required flexibility and ease of installation that is needed for large scale implementation of such a system.

In this work we present a novel fingerprinting-based positioning technique that mitigates the need for the time-consuming offline phase. We take advantage of the VLC data transmission capabilities of the luminaires, to transmit information on lighting configuration inside the room and LED parameters to the user's device, once he enters the room. Based on the transmitted parameters, the mobile device calculates a reference map of directional light intensity distributions in dependence of the location of the room by using a simplified analytical formalism of the illumination pattern of the luminaires and the computational power of a smart phone device. This system requires a receiver capable of discriminating light impinging on the device from different directions. These types of receivers are referred to as angle diversity receivers (ADR).

3.2 Angle diversity receivers

Many different types of ADRs have been reported in literature. He et al. group these ADRs into three categories [37]:

1) ADRs in which photodiodes are mounted on a three-dimensional structure so that they face in different directions.
2) ADRs which consist of an array of photodiodes that face the same direction and lenses are used to direct light from different directions onto different photodiodes.
3) Angular diversity aperture receivers (ADAs) in which photodiodes face the same direction and light from different directions is directed onto different photodiodes using apertures.

The first category of ADRs works with inclined receiver [38] in order to measure the AOA of the incident light. A practical approach to achieve these configurations are pyramidal, hemispherical or cubic geometries where the PDs are placed on the outer surface [39, 40, 41, 42]. The second category uses optics such as spherical lenses in the receiver setup for an imaging system [43] or uses an array of prisms to achieve angular diversity within a compact receiver setup as shown in [44, 45]. The third category uses apertures in combination with PDs. It brings the advantages of a compact design that is capable to get the AOA information of the incident light and are compatible with simple manufacturing techniques. The setup consist of an array of PDs and an array of apertures placed above with a defined lateral shift of each individual aperture with respect to the positions of the PDs. This is discussed in detail in [37, 46, 47, 48] for VLC and VLP, respectively. In [49] it is theoretically shown that centimeter accuracy can be achieved, but will be degraded by system imperfections, like deviation in sizes, shapes and positions of the PDs and differences in dc-offsets at the transmitter and receiver. A similar but more stable approach that reduces these constraints uses only one aperture in combination with a quadrant PD with closely matched quadrants. Quadrant angular diversity aperture (QADA) receivers are used in VLP. With this setup, positioning information can be derived from the light intensity impinging on the quadrant PD [50, 51]. It also has been shown that the setup is extremely sensitive to fabrication imperfection. To overcome this constraints a QADA-plus configuration were introduced and

discussed in [52, 53], where the two-stage system combines the QADA with a camera and taking advantage of both receiver types.

However, in this study the receiver unit consists of an array of photodiodes where each photodiode only detects light from an defined allocated azimuthal angle interval. The whole azimuthal FOV (0 to 360 deg) is divided into equidistant angular segments, which depend in their size on the number of photodiodes, e.g. an array of 4 photodiodes results in 4 angular segments each of which spans 90° of the azimuthal angle so that the whole azimuthal FOV is covered. We refer to this kind of receiver as an angular segmented receiver (ASR). The idea of using angular segmented receiver designs for indoor wireless optical communication systems was first introduced in [54]. In this work the authors introduce a hemispherical receiver design where the region between two parallel meridians is referred to as segment Each sector consists of an optical entrance surface with a field of view specified by two limiting azimuth angles and the two limiting polar angles, and the associated front-end and control circuits [54].

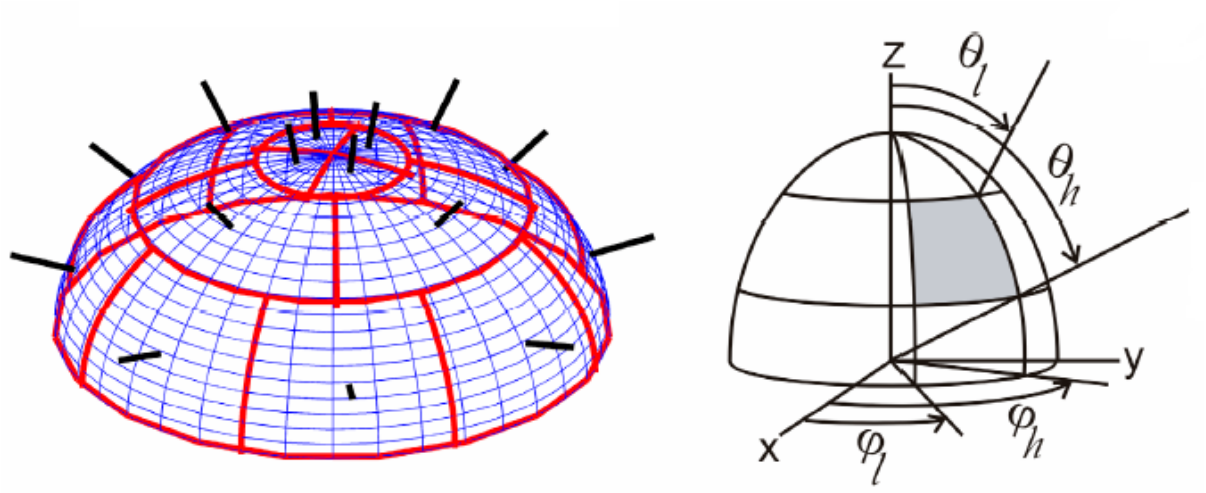

Figure 11 Adopted from [55]. Hemispherical sectored angle-diversity receiver proposed in [V2]. Each sector is specified by the two limiting azimuth angles φ_l and φ_h and the two limiting polar angles Θ_l and Θ_h.

An advantage of an ASR like the one described in Figure 11 [55] is that by separating light by its azimuth angle relative to the receiver, time dispersion is reduced, resulting in higher bit rates for VLC and being able to determine the AOA of the incident light, which can be used to determine the position data. This feasibility study investigates the 2D positioning

capabilities of an angular segmented receiver and analyzes the tradeoff between number of segments and receiver size. While a higher number of photodiodes, and the associated finer angular resolution will result in better positioning accuracy, a higher number of photodiodes also leads to a bigger physical receiver unit. A device too big in size would defeat the purpose of a comfortable wearable device or use in a smartphone. We utilize ray tracing techniques for simulating realistic angular intensity distributions inside a specified indoor environment and self-developed MATLAB algorithms for assessing receiver configuration and system performance.

3.3 Description of the simulation setup

In order to realistically simulate the intensity distribution over the entire azimuthal angle at distinct positions inside the investigated room scenario, we use again the commercial software ASAP (Breault Research Organization) which is capable of performing non-sequential Montecarlo ray-tracing simulations.

For the ray tracing simulations, we apply the VLC channel model described in section "2. VLC Channel Modelling". The simulated room has dimensions of 5 m x 5 m x 3 m with four luminaires L1-L4 on the ceiling, each consisting of 100 LED chips. Each LED emits with a radiant power of 0.45 W and has a Lambertian radiation characteristic confined to a cone angle of 120°. We modelled the LED dice as square-shaped, light-emitting surfaces, which were modified in their radiation characteristics to meet all the desired parameters, summarized in Table 3.

Table 3 Parameters of the simulation setting.

Size of room	5[m] x 5[m] x 3[m]
Time Resolution	0.2 [ns]
Number of luminaires	4
Number of LED dice per luminaire	100
Number of rays for each die	400000
Radiant power of each die	0.45 [W]
Luminaire positions	(1.5,1.5,3) [m] (1.5,3,3) [m] (3.5,1.5,3) [m] (3.5, 3.5,3) [m]
Cone angle of LED emission	120°
Field of view of receivers	60°
Area of receivers	1 [cm^2]
Scattering model	Lambertian Scattering

The spectral power distribution (Fig. 3a) of the LED emission was modelled with 13 sample points and is based on a commercially available LED (Cree Xlamp MC-E White LED). It is identical to the spectral power distribution used in section "2. VLC Channel Modelling" of this work. To ascribe spectral reflectivity values (Figure 12 b)) to the four room walls, a small sample of white wall paint was measured in the integration sphere setup of a Lambda 900 spectrometer from Perkin-Elmer. Spectral reflectivity values of ceiling and floor were adopted from the measurement values provided in [27].

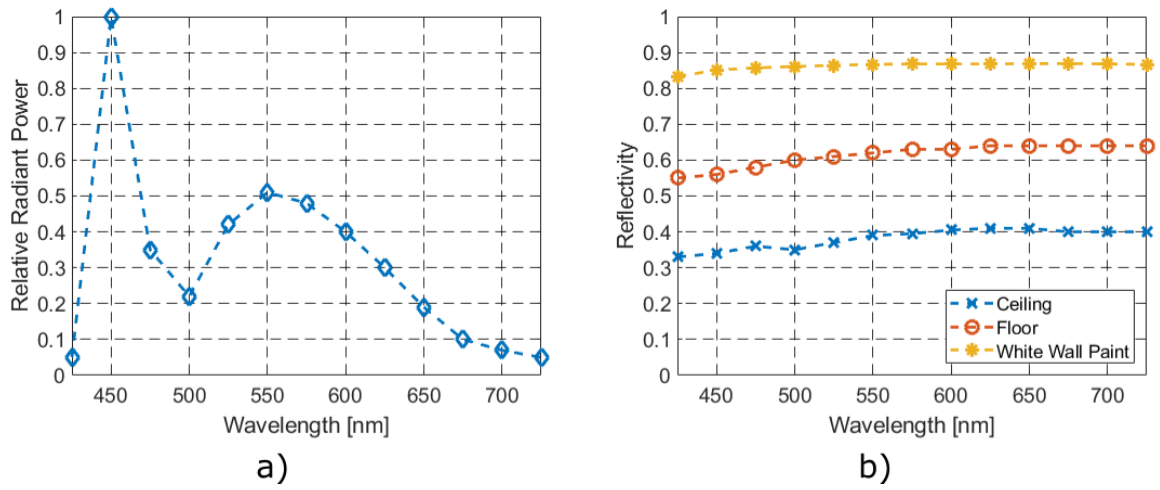

Figure 12 a) Relative spectral radiant power used for modelling the LED chips in the luminaires. b) Spectral reflectivity values for ceiling, floor and white wall paint.

To take into account the diffuse scattering properties of these surface materials, e.g. white plaster of a room wall, in the simulation model we use the Lambertian scattering function which is implemented in ASAP.

The area of receivers is modelled as a fully absorbing surface, 1 cm^2 in size. As described in chapter "2.3 Methodology", we again use the channel modelling method where an output file is generated by the ray-tracing software and passed to Matlab. When a ray hits a fully absorbing receiver surface, the ray is stopped and is no more traced further on. Rays that do not reach a receiver unit before, are either stopped after reaching a user defined, fixed number of allowed reflections, or by setting a minimum threshold for the flux that is carried by a ray. As demonstrated by Miramirkhani et al. in [27], there was no noticeable change in channel characteristics, e.g., received power or time dispersion parameters, for a maximum number of reflections set to 4 or larger within the investigated scenario. Therefore, the maximum number of times any ray may be reflected is fixed to 4 in this study.
In order to simulate a realistic light intensity distribution in the different angle segments of the receiver device, we perform ray-tracing simulations, in the scenario described above (Table 3, Figure 12). We investigate the light intensity distribution over the azimuthal angle at different receiver positions in the horizontal plane 1.5 m above the floor. We chose this height for the receiver plane, because 1.5 m is about the height at which a wearable device would be placed on the shoulder of an average person. This plane is sampled with 81 receiver positions, which are arranged in a rectangular grid with 0.5 m distance between each position (see Figure 13).

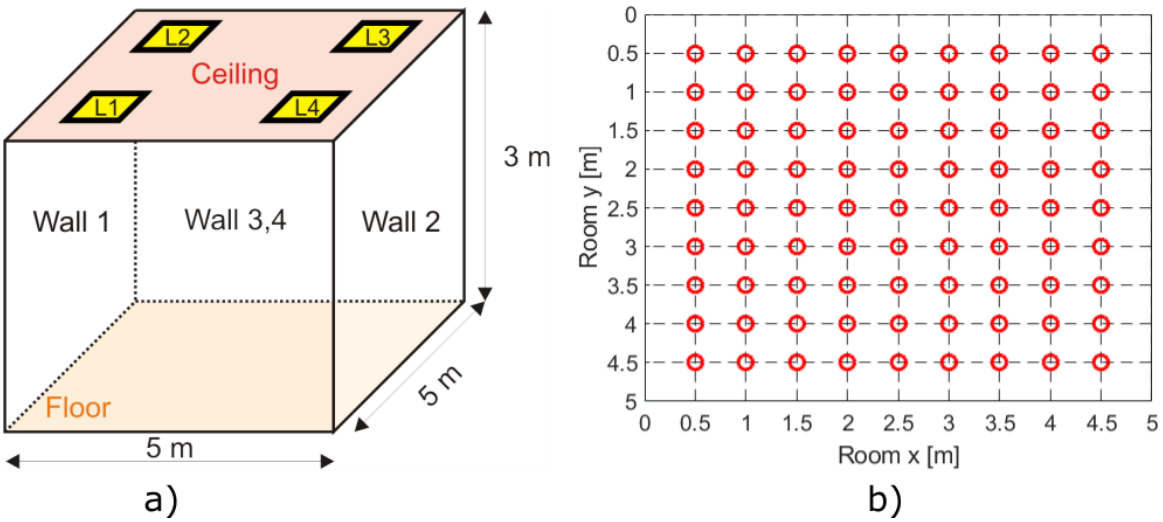

Figure 13 : a) Model of simulated 5 m x 5 m x 3 m room with four luminares L1-L4 on the ceiling. b) Simulated receiver positions in the horizontal plane 1.5 m above the floor.

The orientation of the receivers is chosen in such a way that the first angular segment is centered at 0°. In the example given in figure 14, 4 angular segments are shown. The first segment is centered at 0° therefore the 90° span of this segment lies between 315° and 45°.

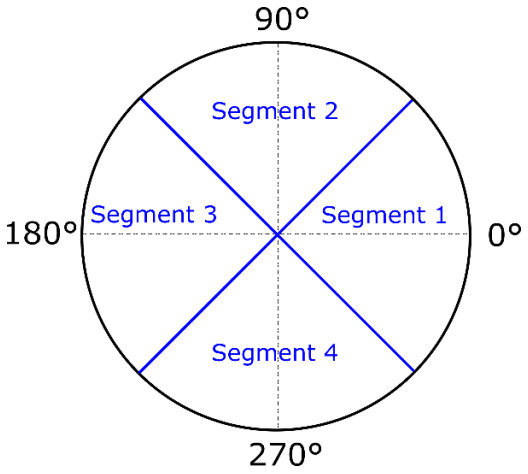

Figure 14 Orientation of the receivers inside the room. The first segment of any receiver is always centered at 0°. In this example of 4 angular segments the resulting angle intervals are as follows: Segment 1 from 315° to 45°, Segment 2 from 45° to 135°, Segment 3 from 135° to 225°, Segment 4 from 225° to 315°.

In order to safe simulation time, we take advantage of the simulation technique described in chapter "2.6.1 Simultaneous simulation of variable receiver positions along a defined path" where we deployed many receiver positions simultaneously in one simulation run. We follow the same principle here and therefore all 81 receiver positions are deployed simultaneously, so there is no need for 81 individual time-consuming simulation runs to cover all receiver positions. An artificial simulation error can be expected, when simulating 81 receiver

positions at once, because a ray that hits one of the absorbing receiver positions, is stopped there. However, it could have been reflected of the room surface, and after another reflection at the wall, it could hit another receiver position in the room. We are confident that this artificial simulation error is negligible, considering all 81 receivers deployed simultaneously account for only 0.03% area of the 25 m^2 room floor. The characteristics of the rays, that reach a receiver surface, are logged into a file containing all relevant information about these rays, such as location, direction, flux, optical path length, number of object intersections and wavelength. A full list of information that can be deducted from a ray can be seen in talbe 1. This list of ray characteristics is forwarded to MATLAB for further analysis. The division of the rays according to their azimuthal angle is done in MATLAB, based on their x and y directions. This method of analysis offers the flexibility to choose any desired number of angle segments from the same data set, after the simulations have ended without the need for additional time-consuming simulations. Since the light sources are modelled to emit light in a cone angle of 120°, the highest possible polar angle of incidence for direct light is 60°. Light with polar angle of incidence of more than 60° is light reflected from the walls. From Figure 10 it is apparent that most light is concentrated in azimuthal angles of 60° or lower. For this reason we assume a polar FOV of 60° for receivers to reduce the influence of stray light.

3.4 Statistical error estimation of the ray tracing technique

In this paper we investigate the room described in [56] for 3 configurations of different wall reflectivity values. The standard case uses the measurement values of the white paint (Figure 12 b)). The second configuration uses walls that have exactly half the reflectivity values of the measurement values depicted in figure 12 b). In the third configuration, all 4 walls are fully absorbing.

To assess the statistical error, due to a finite number of rays used in Montecarlo ray-tracing, we simulate each of the three scenarios described above four times. In every simulation run, each LED chip emits 400k rays, resulting in 160 million rays overall. On each of the 81 receiver positions, we calculate the channel DC gain (H), mean excess delay (τ_0) and root

mean square delay (τ_{rms}) and calculate the standard deviation (SD) of these characteristics between the four individual simulation runs. In Table 2, the averaged values along the corresponding averaged standard deviations of the channel characteristics over all 81 positions are listed. As one can see from this table, there are small but non-negligible deviations in channel characteristics, that should be taken into account when assessing or calculating channel characteristics.

Table 4 Average channel characteristic, Channel DC gain (H), mean excess delay (τ_0) and root mean square delay (τ_{rms}), and their average standard deviation (SD), calculated from 4 individual simulation runs for each scenario.

Wall Reflectivity	H average [W]	SD(H) average [W]	τ_0 average [s]	SD(τ_0) average [s]	τ_{rms} average [s]	SD(τ_{rms}) average [s]
White paint	1.7e-4	1.9e-6	9.9e-9	1.3e-10	9.8e-9	1.8e-10
Half of white plaster	1.5e-4	1.9e-6	8.0e-9	8.4e-11	6.9e-9	1.7e-10
Absorbing	1.5e-4	1.8e-6	6.9e-9	5.9e-11	4.4e-9	1.7e-10

3.5 Proposed VLP system overview

In this study we propose to use a receiver which consists of an array of photodiodes which can resolve light from different azimuthal angles by means of an upstream optical system. The approach for Visible Light Positioning by fingerprinting described in this work, has the advantage of not requiring real life measurements in indoor environments where positioning is desired. Figure 15 describes the basic concept of our approach.

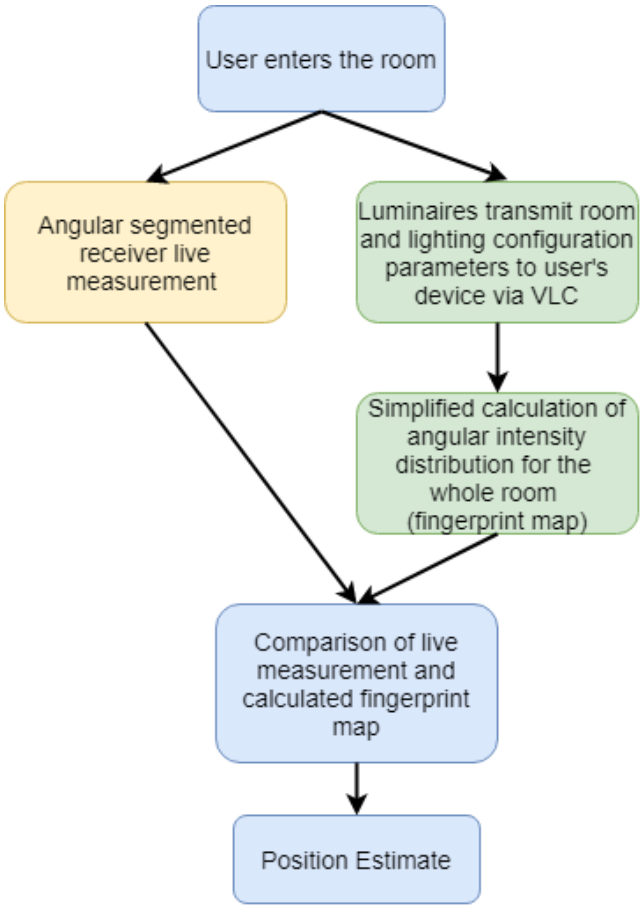

Figure 15 Block diagram of the proposed system. A user enters the room, with a device which is equipped with an angular segmented receiver, which measures the light intensity in every angular segment. Once the user enters the room, the luminaires transmit to the user's device information on the room configuration and lighting parameters via VLC. With this information the user's device calculates a simplified angular intensity distribution for the whole room, which serves as the reference data set for fingerprinting.

We take advantage of the VLC data transmission capabilities of the luminaires, to transmit information on lighting configuration inside the room and LED parameters to the user's device, once he enters the room. Based on the transmitted parameters, the device calculates a theoretical light distribution in the segments within this room. The map of calculated light distributions serves as the reference data set for fingerprinting, bypassing the need for an offline phase with real world measurements. As follows, the calculations are relatively simple and do not require high computing power. It can be assumed that a utilized smart device, such as a smartphone, has sufficient computing power to perform these calculations on its own. By transmitting to the user

- Room dimension
- Position, dimension and number of the luminaires
- Radiation pattern of the LEDs or the luminaires (from e.g. datasheets)

the user's device is able to calculate the expected light intensity in every solid angle for each LED chip. Assuming Lambertian radiation patterns the integral

$$I = \int_{\varphi 1}^{\varphi 2} \int_{\theta 1}^{\theta 2} \cos(\theta) \sin(\theta)\, d\varphi\, d\theta \qquad (1)$$

gives the intensity in every solid angle element covered by the receiver unit. The integral is conducted for every LED chip of the luminaires considering their individual position and assuming a point sources with a Lambertian radiation characteristic. If the radiation pattern of the source deviates too much from Lambertian pattern, an additional angle dependent weighting function has to be considered in the integral to take account of this deviation. In this case, this information should be part of initial transmitting process. This fingerprint map is calculated without taking into account any wall reflections, so that the computational effort stays low. The result is a calculated map of the room that contains information on radiant flux per solid angle in a horizontal plan at a certain height above the floor. In our paper we focused on a height of 1.5 m, which is approximately the height at which a portable device would be placed on the shoulder of an average person. We calculated the fingerprinting map with a resolution of 10 mm in both dimension of the plane. To ensure comparability between calculated values (fingerprinting map) and measured values both values must be normalized to the overall radiant flux impinging on the receiver. In our contribution, we emulate the measured values by ray-tracing simulation taking into account realistic yet simplified optical properties of the room setup. In our approach, the device will calculate the absolute difference of measured values in every angular segments and every sample point in the calculated reference map. The sum of deviations of intensity in every angular segment is used as a measure for the probability of the actual position in the room. To obtain an estimate of the current position, the position with the smallest deviation from the fingerprinting map for the position estimate is used. Should there be more than one position in the calculated fingerprinting map with the same numerical value for difference, the algorithm calculates from these positions, a mean x value and a mean y value for current position estimate.

In figure 16, an example for this procedure is given for the room scenario with white painted walls and an ASR with 12 angular segments. Figure 16 a), b), and c) are examples for illustrating the positioning estimates in dependence of the actual position inside the room,

marked by either a green cross or a red circle, respectively. The absolute difference between the simulated ray-tracing values for intensity in the angular segments and the values from the calculated reference map is indicated by the color coding, where blue means a small and yellow a high deviation. In Figure 12 d) the the positioning error for all receiver positions across the room is depicted, where each color-coded pixel corresponds to the positioning error at the corresponding location.

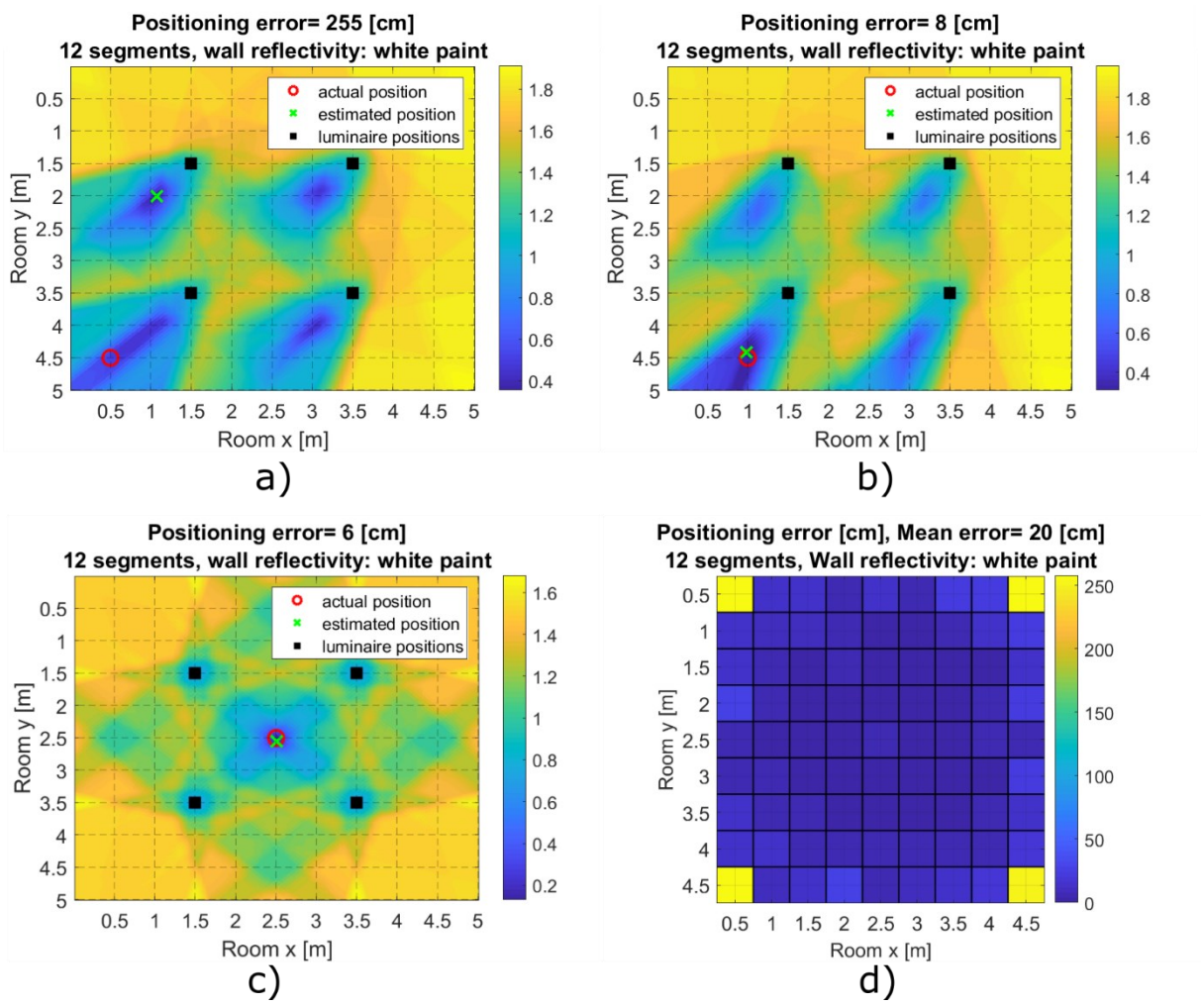

Figure 16 Actual position and estimated position inside the room for a receiver unit consisting of 12 angular segments and wall reflectivity of white paint. The color bar on figure 2 a)b)c) indicates the absolute difference between the normalized ray tracing intensity distribution for the actual position and the normalized intensity distribution at every position in the fingerprint map a) Position estimate at position x=0.5 m, y=4.5 m with a large error due to the strong influence of the reflected light which is high in the corner of the room, b) position estimate at position x=1 m, y=4.5 m, c) position estimate at position x=2.5 m, y=2.5 d) Positioning error for all 81 sample points inside the room. Each color-coded pixel in the error map corresponds to one of the 81 sample positions. The value besides the color scale corresponds to the position error in centimeter.

3.6 Results

We calculate the positioning error under consideration of different scenarios of 3 different room setups by varying the reflectivity of the four walls according to description above and Fig. 4b. For the investigation of these scenarios the number of angular segments for the receiver unit is varied. Starting with 4 azimuthal angular segments and increasing the number of segments by 4 in each iteration up to 24 segments.

Depicted in Figure 17 are the positioning errors using ASRs with varying number of segments under the assumption that the room has white painted walls. The same figure arrangement is depicted for half reflectivity values and absorbing walls in Figure 18 and Figure 19 respectively. Each color coded pixel in this figure corresponds to one sampled position inside the room. The color of a pixel corresponds to the positioning error, in regards to difference between actual position inside the room and the position estimate, made by our position estimation method. It has been shown that an increase in the number of segments leads to better positioning results. Increasing the number of segments from 4 to 24 resulted in an improvement of the average positioning error from 79 cm to 5 cm in this configuration. The relatively high average value for the error can be attributed to the problem zones near the corners of the room.

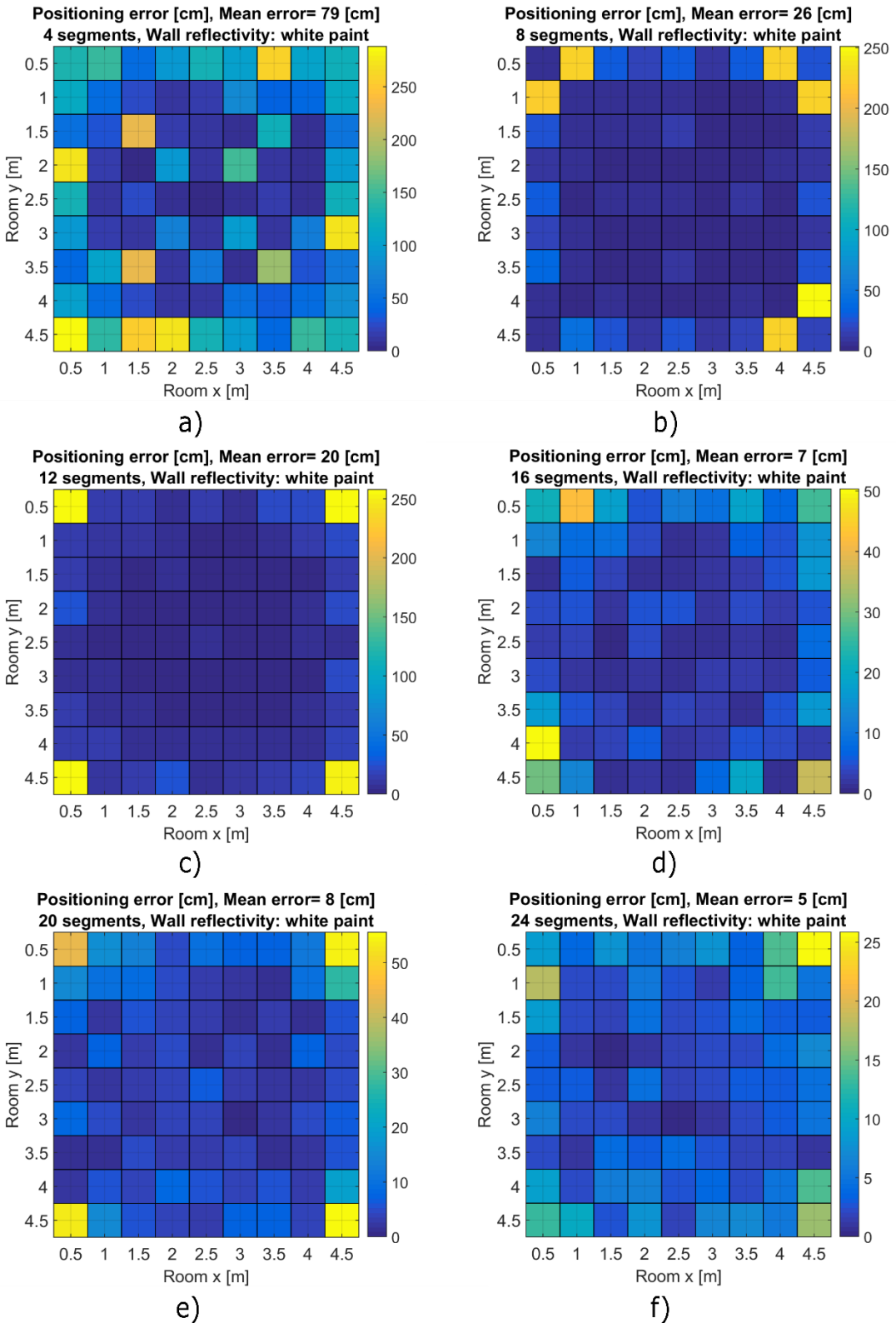

Figure 17 Positioning error maps for the scenario considering white-painted walls. Each pixel corresponds to one position inside the simulated room. a) Error map for 4 angular segments. Mean positioning error= 79 cm b) Error map for 8 angular segments. Mean positioning error= 26 cm c) Error map for 12 angular segments. Mean positioning error=20 cm d) Error map for 16 angular segments Mean positioning error=7 cm e) Error map for 20 angular segments. Mean positioning error=8 cm f) error map for 24 angular segments. Mean positioning error=5 cm.

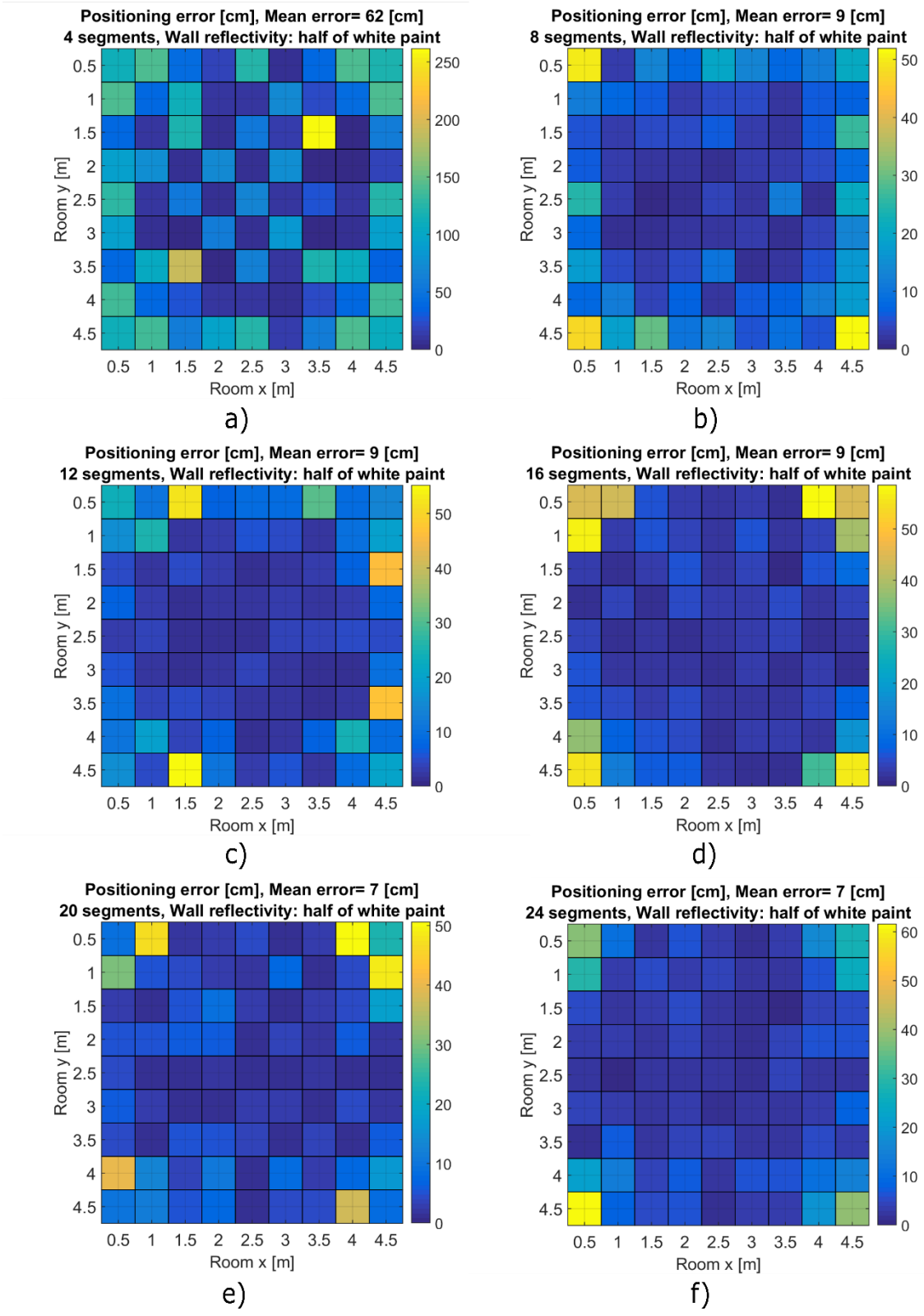

Figure 18 Positioning error maps for the scenario considering walls with half the reflectivity values of white paint. Each pixel corresponds to one position inside the simulated room. a) Error map for 4 angular segments. Mean positioning error= 62 cm b) Error map for 8 angular segments. Mean positioning error= 9 cm c) Error map for 12 angular segments. Mean positioning error=9 cm d) Error map for 16 angular segments Mean positioning error=9 cm e) Error map for 20 angular segments. Mean positioning error=7 cm f) error map for 24 angular segments. Mean positioning error=7 cm

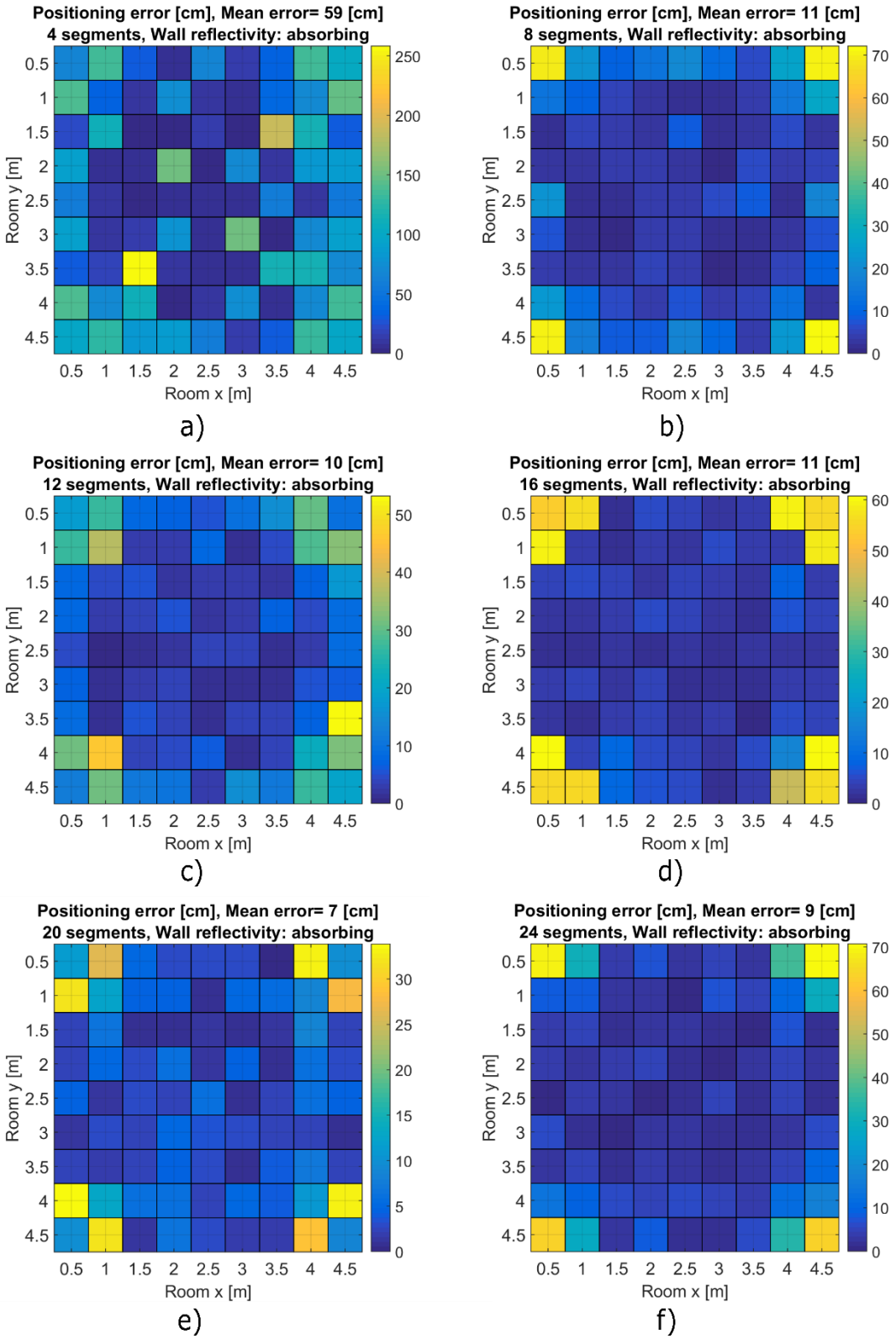

Figure 19 Positioning error maps for the scenario considering absorbing walls. Each pixel corresponds to one position inside the simulated room. a) Error map for 4 angular segments. Mean positioning error= 59 cm b) Error map for 8 angular segments. Mean positioning error= 11 cm c) Error map for 12 angular segments. Mean positioning error=10 cm d) Error map for 16 angular segments Mean positioning error=11 cm e) Error map for 20 angular segments. Mean positioning error=7 cm f) error map for 24 angular segments. Mean positioning error=9 cm.

Table 5 shows the average positioning error over all 81 receiver positions in dependence of the number of angular segments and the reflectivity of the walls, in the simulated setting. From Figure 17, Figure 18 and Figure 19 it is apparent that the large values for average positioning error in Table 5 are strongly influenced by the relatively high positioning errors near the walls, and in particular in the corners of the room. It would be expected that a reduction in wall reflectivity would be accompanied by an improvement in positioning accuracy, since the fingerprint map is calculated without taking into account any wall reflections. By not including any wall reflections in the calculation of the fingerprint map, the model complexity and computational effort stays low. This effect could not be confirmed in its general validity, since table 5 shows the increase in positioning error for reduced wall reflectivity, e.g. for 16 angular segments.

Table 6 shows the positioning errors for all scenarios, excluding all positions all positions along the walls of the room. If these positions are excluded from the calculation of the mean value, the positioning errors for all room configurations are greatly improved e.g. for 4 angular segments for the white paint setup the value droops the mean error from 79.3 cm to 44.4 cm. This can be explained by the fact that near highly reflective walls there is an increased influence of scattered light, which gives reason for a misinterpretation of the position in the algorithm.

Table 5 Average positioning error for three simulation scenarios in dependance of the number of angular segments for the receiver unit.

Wall reflectivity	**Number of angular segments**					
	4	8	12	16	20	24
White Paint	79.3 cm	25.6 cm	20.0 cm	7.3 cm	7.8 cm	4.8 cm
Half of white paint	61.8 cm	9.0 cm	8.8 cm	9.1 cm	7.4 cm	7.0 cm
Absorbing	59.3 cm	10.5 cm	10.0 cm	11.3 cm	7.8 cm	9.1 cm

Table 6 Average positioning error, without receiver positions in the edge areas near the walls of the room, for three simulation scenarios in dependence of the number of angular segments for the receiver unit.

Wall reflectivity	Number of angular segments					
	4	8	12	16	20	24
White Paint	44.4 cm	3.8 cm	4.0 cm	3.3 cm	4.0 cm	3.0 cm
Half of white paint	43.3 cm	4.0 cm	4.4 cm	3.2 cm	3.7 cm	3.7 cm
Absorbing	47.0 cm	4.5 cm	5.8 cm	3.5 cm	4.2 cm	3.8 cm

3.7 Discussion

To gain better insight on why large positioning errors tendentially occur for lower number of angular segments, near the walls and especially in the corners of the room, we compare two sets of figures for one representative receiver position near the walls at x=0.5 m and y=2.5 m. For every number of angular segments, Figure 20 a) to f) shows the positioning error that results at this receiver position. Depicted in figure 21 are the corresponding relative intensity distribution of incident light on the receiver, depending on the azimuthal angle and the number of angular segments. These visualizations are interpreted as what the receiver "sees". In the case of 4 angular segments (Figure 21 a)) the algorithm misinterprets the position, as most of the light falls in the first segment centered at 0°. Therefore, algorithm interprets the angular light distribution in figure 21 a) as one that occurs to the left of luminaries. The reason the position next to the particular luminaire positioned at x=1.5 m and y=3.5 m was chosen, depends on statistical uncertainties of the ray tracing method. Better position estimates result from more angular segments. In the example of 8 angular segments in figure 21 b) , one can see that 2 of the 8 segments, which point towards the two nearest luminaires receive almost all intensity. In this case and cases with more angular segments, the position estimates of the algorithm come closer to the actual position.

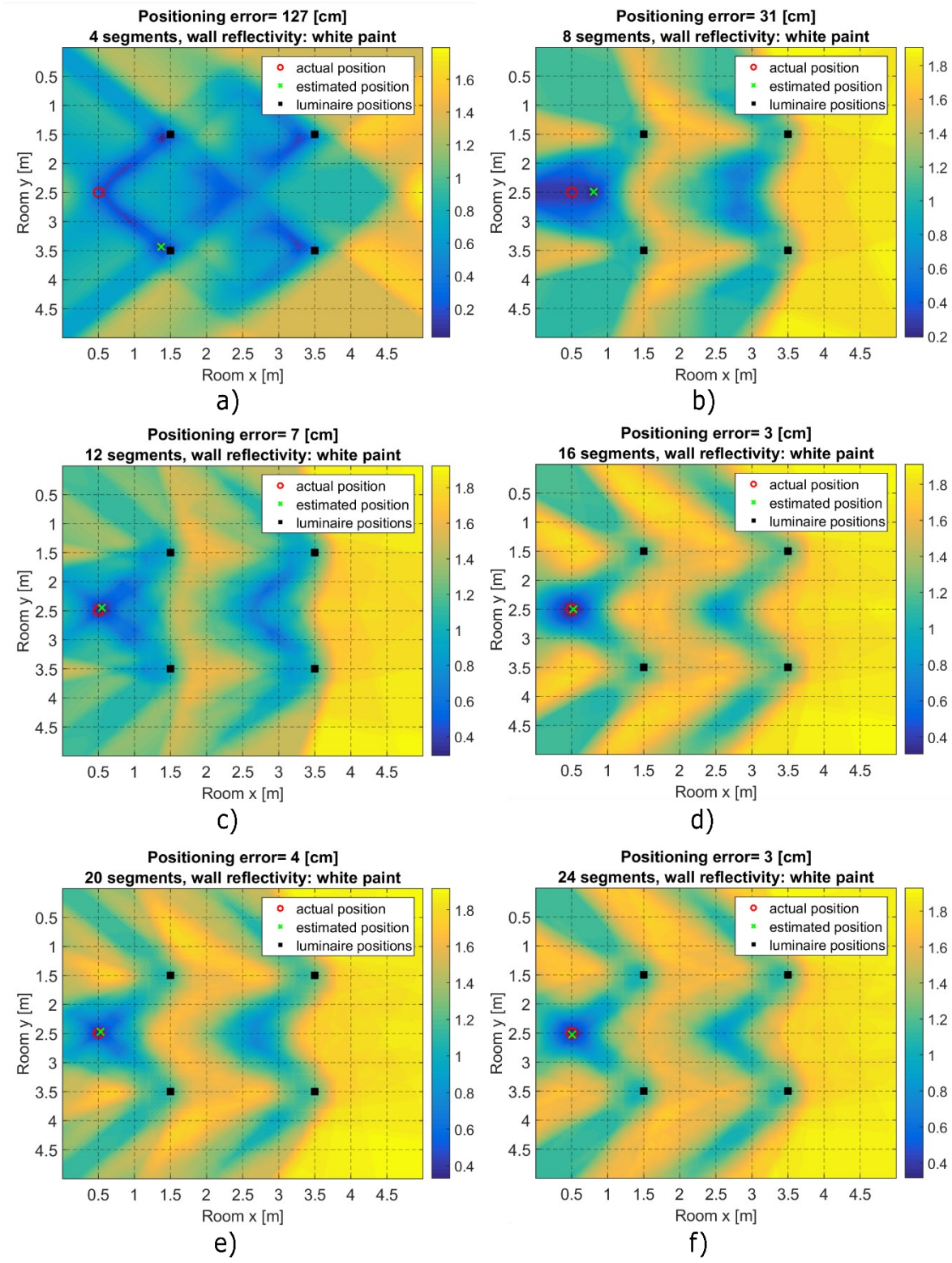

Figure 20 Comparison of positioning estimates at the room position x=0.5 m & y=2.5 m under the variation of angular segments used for light detection. Positions near the walls are prone to relatively large positioning errors. a) 4 angular segments. Positioning error= 127 cm. b) 8 angular segments. Positioning error= 31 cm. c) 12 angular segments. Positioning error= 7 cm. d) 16 angular segments. Positioning error= 3 cm. e) 20 angular segments. Positioning error= 4 cm. f) 24 angular segments. Positioning error= 3 cm.

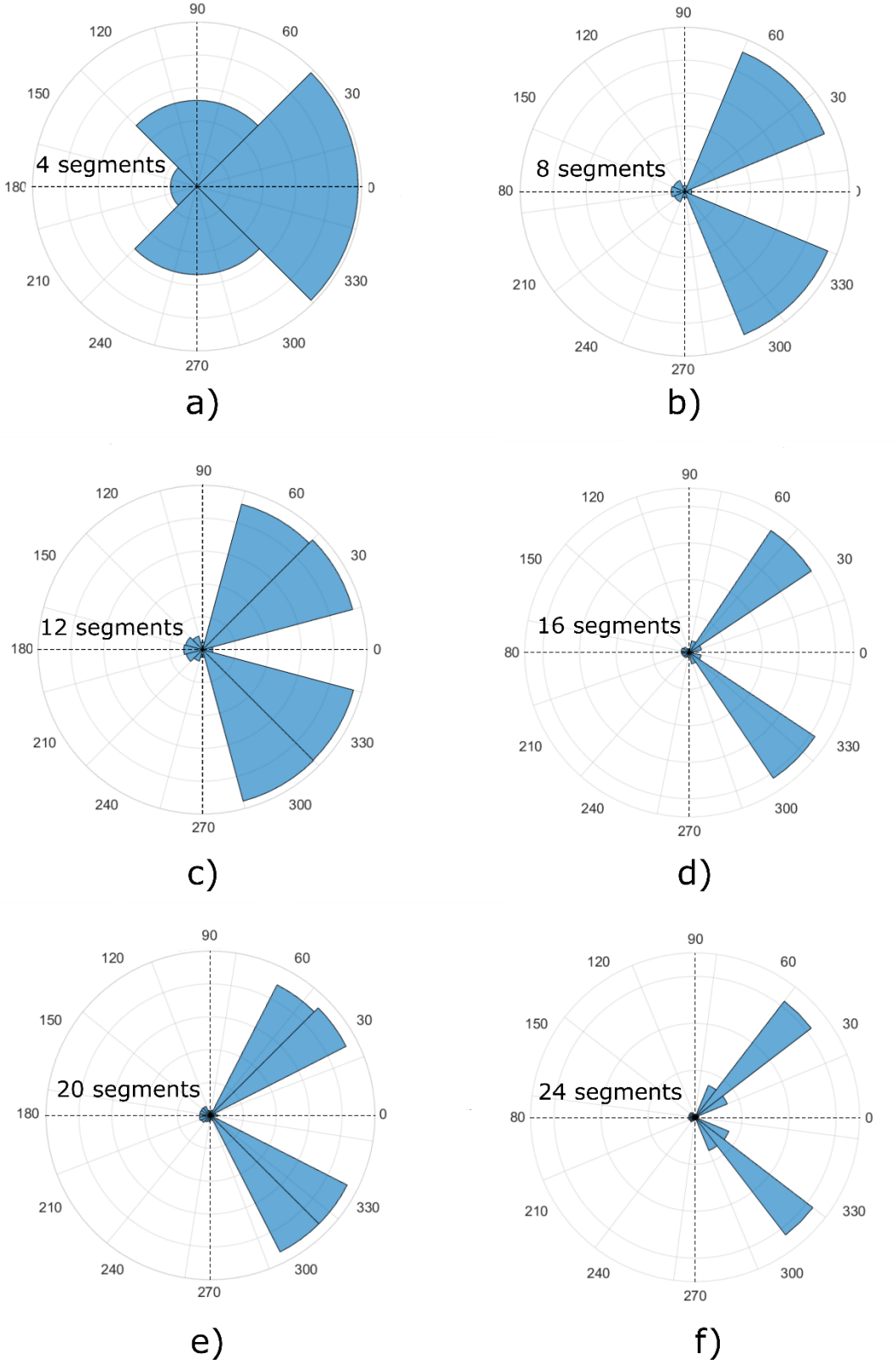

Figure 21 Visualization of the relative intensity distribution of incident light in dependance of the azimuthal angle at receiver position x=0.5 m & y=2.5 m. a) 4 angular segments b) 8 angular segments c) 12 angular segments d) 16 angular segments e) 20 angular segments f) 24 angular segments.

As mentioned above, reflections from the wall lead to worse positioning estimates since the theoretical fingerprint map is calculated without accounting for wall reflections. The example in Figure 22 at receiver position x=4.5 m and y=4.5 m shows how this can lead to relative high positioning errors. In figure x a) you can see that the actual position is located in the corner of the room and the algorithm estimates the position to be near the luminaire approximately at x=3.6 m and y=3.6 m. Figure 22 b) is the relative intensity distribution the receiver "sees" at the actual position. The intensity in the angular interval between 225° and 45° comes purely from reflected light. Figure 22 c) and d) are the receiver measurements at position x=4 m and y= 4 m and x=3.5 m and y=3.5 m respectively. Since the algorithm does not account for reflections from the walls the position is estimated to lie inbetween these two positions where a similar intensity distribution pattern is expected, due to the direct light coming from the luminare.

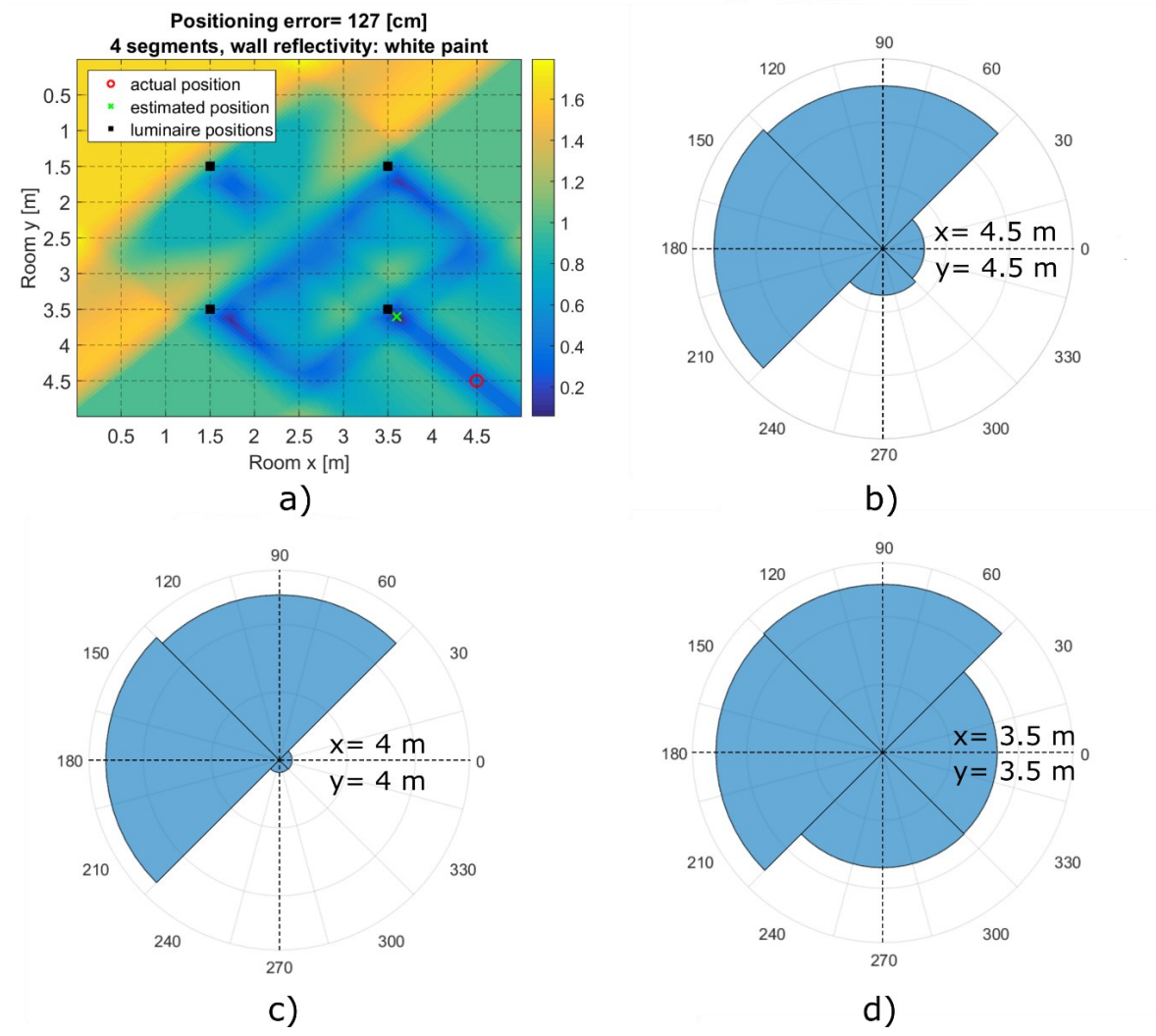

Figure 22 Positioning estimate for 4 angular segments at room position x=4.5 m y=4.5 m. a) receiver measurement at the actual position x=4.5 m & y=4.5 m. The intensity in the angular interval between 225° and 45° comes purely from reflected light. Since the algorithm does not account for reflections from the walls the position is estimated to be between x=4 m & y=4 m & x=3.5 m & y=3.5 m where a similar intensity distribution pattern is expected. b) receiver measurement at position x=4 m & y=4 m. c) receiver measurement at position x=3.5 m and y=3.5 m.

3.8 Reduction of multipath dispersion

As shown in [57], it is possible to reduce the multipath dispersion in the optical wireless channels by using segmented receivers. The authors in [57] propose two possibilities to select an angular segment of the ASR to use for data communication. The first possibility, "lowest time dispersion" selects the segment with the lowest root mean square delay spread (τ_{RMS}) since τ_{RMS} is inversely proportional to the maximum achievable bit rate. The other possibility "highest intensity" selects the angular segments using a criterion independent of the channel impulse response, in our case the segment with the highest channel DC gain is selected. In table 5 we show the average τ_{RMS} values for all 81 receiver positions inside the room for an unsegmented receiver in comparison to the investigated angular segmentations of receivers. An improvement in τ_{RMS} along an increasing number of angular segments is to be expected and is in accordance with the findings in [57]. For example, the receiver with no angular segmentation (0 segments) measures a root mean square time dispersion of 9.8 ns. Introducing 4 angular segments and selecting either the segment with the lowest time dispersion or the highest intensity, the root mean square delay drops to 6.8 ns. These values are summarized in Table 7.

Table 7 Average improvements in time dispersion over all 81 receiver positions in dependence of the number of angular segments. In the middle column segments with the lowest time dispersion are selected. The right column selects segments with the highest channel DC gain.

Number of angular segments	τ_{RMS} [ns] (lowest time-dispersion segment)	τ_{RMS} [ns] (highest intensity segment)
0	9.8	9.8
4	6.8	6.8
8	5.8	5.9
12	4.9	5.0
16	4.6	4.8
20	4.3	4.4
24	4.1	4.4

3.9 Future Work

This study examines the advantages and 2D positioning capabilities of an ASR in combination with a theoretically calculated reference map for visible light positioning, which is based on the directional light distribution on distinct positions in the indoor scenario. As pointed out in [33] the performance of a fingerprinting based VLP system is heavily reliant on the algorithm used to classify the current signal based on the reference fingerprint map. We recognize the possible application of machine learning algorithms for pattern recognition for the positioning system proposed here.

For testing the proposed system in a real-world setup, the front-end optics for an ASR need to determined. The light can be directed into the designated angle segments by using freeform lenses or other light-directing elements. We also report the possibility to introduce additional angle segments which do not distinguish light by its azimuthal angle, but by its polar angle. By doing this we expect to obtain height information and therefore to extend the approach presented in this paper from 2D positioning to 3D positioning.

Tilt, receiver orientation and shadowing effects are yet to be considered in the future. Different works have been reported that combine accelerometer measurements with VLP techniques in order to gain information on receiver attitude. Yasir et al. address the issue of receiver attitude by using accelerometers to measure attitude of the receiver, which provides an angle estimation for their AOA triangulation positioning [58]. The integration of our ASR receiver for example in the compact sensor board NGIMU (x-io technologies) is left as future work. The NGIMU unit includes a triple-axis gyroscope, accelerometer and magnetometer, which can be used for receiver-attitude information.

4. Conclusion

The first section of my work deals with channel modelling in Visible Light Communication. Ray-tracing based channel modelling is a powerful tool for the determination of the channel characteristics of VLC settings. By exporting a file containing relevant information on each ray as determined by ray-tracing, it is possible to do further analysis of the investigated setting without the need for additional ray-tracing simulation runs. In this regard, we have presented a channel model that is based on optical simulations using non-sequential ray-tracing in combination with self-developed algorithms in MATLAB. We introduced an approach, which allows the determination of the dependence of the receiver position on the VLC characteristics along the diagonal of the floor of a room. Ray information of each ray impinging on this diagonal stripe (with a width of ~1.41 cm) is exported to MATLAB for further analysis. By doing so, many investigations can be performed ex post and do not require additional time-consuming ray-tracing simulation runs. In the present investigation, 26 different receiver positions along the diagonal axis of a room were investigated using only one wavelength dependent simulation sweep instead of 26 independent simulation sweeps for achieving similar results when considering just one single position of the receiver unit. The error made by this simulation approach was estimated to be negligible because of the small ratio between detector stripe area and the area of the whole floor surface.

In the second half of this thesis, we have proposed to use angular segmented VLC receivers in combination with a novel fingerprinting technique for indoor 2D positioning. The main disadvantage of fingerprint positioning techniques is reported to be the high time effort, due to the need for real-world sample measurements in every room where positioning is desired [58]. We address this issue by taking advantage of VLC capabilities of the luminaires inside the room to transmit to the mobile user information on the room and lighting configuration therein. With this information the user's device which is equipped with an ASR, calculates a map of theoretical light intensity distribution in the different segments of the ASR depending on the position in the room. Alternatively, a locally stored copy of this map could be transmitted to the mobile user. By comparing the current light distribution impinging on the

receiver unit with predicted light distributions inside the room from the calculated map, the best match for the current position is determined.

We utilize ray-tracing techniques to simulate realistic light intensity distribution on 81 distinct receiver positions arranged in a rectangular grid 1.5 m above the floor of a 5 m x 5 m x 3 m room, applying the channel model and simulation techniques described in chapter "2.6.1 Simultaneous simulation of variable receiver positions along a defined path". Based on these simulated light distributions, the algorithm estimates the current position by comparing the current distribution with the theoretical distributions calculated with the parameters which are transmitted from the luminaires to the user's device via the wireless optical channel. In our simulations, the system achieves centimeter-level accuracy inside the room.

Another advantage of using ASRs in VLC systems is the reduction of multipath dispersion in the optical channel. By either selecting the angular segment of the ASR with the highest intensity or the lowest time dispersion for data transmission, we have shown that the time dispersion decreases compared to an unsegmented receiver. This results in an increase of the maximum achievable bit rate.

5. Acknowledgement

The authors gratefully acknowledge the part-financing of the project by the Federal State of Austria, the Province of Burgenland and the European Regional Development Fund in the context of the Investment for growth and jobs goal.

6. References

[1] Clement J. 28.02.2020, Global mobile data traffic from 2017 to 2022, https://www.statista.com/statistics/271405/global-mobile-data-traffic-forecast/

[2] Haas, Harald & Chen, Cheng & O'Brien, Dominic. (2017). A guide to wireless networking by light. Progress in Quantum Electronics. 10.1016/j.pquantelec.2017.06.003.

[3] E. W. Lam and T. D. C. Little, "Visible Light Positioning for Location-Based Services in Industry 4.0," 2019 16th International Symposium on Wireless Communication Systems (ISWCS), Oulu, Finland, 2019, pp. 345-350, doi: 10.1109/ISWCS.2019.8877305.

[4] Al-Kinani, Ahmed & Wang, Cheng-Xiang & Zhou, Li & Zhang, Wensheng. (2018). Optical Wireless Communication Channel Measurements and Models. IEEE Communications Surveys & Tutorials. PP. 1-1. 10.1109/COMST.2018.2838096.

[6] Yahoo News, 25.11.2015 Goodbye Wi-Fi, Hello Li-Fi: New Wireless Technology Is 100 Times Faster, https://uk.news.yahoo.com/wave-bye-bye-wi-fi-083520653.html?guccounter=1

[7] H. Haas, August 2011, Wireless Data from Every Light Bulb, http://bit.ly/tedvlc.

[8] Miramirkhani, Farshad & Uysal, Murat. (2017). Visible Light Communication Channel Modeling for Underwater Environments with Blocking and Shadowing. IEEE Access. 6. 1082-1090. 10.1109/ACCESS.2017.2777883.

[9] D. Feezell, and S. Nakamura, “Invention, development, and status of the blue light-emitting diode, the enabler of solid-state lighting”, C. R. Physique vol. 19, pp. 113–133, 2018

[10] E. W. Lam and T. D. C. Little, "Visible Light Positioning for Location-Based Services in Industry 4.0," *2019 16th International Symposium on Wireless Communication Systems (ISWCS)*, Oulu, Finland, 2019, pp. 345-350. doi: 10.1109/ISWCS.2019.8877305

[11] Do TH, Yoo M. An in-Depth Survey of Visible Light Communication Based Positioning Systems. Sensors (Basel). 2016;16(5):678. Published 2016 May 12. doi:10.3390/s16050678

[12] Y. Zhuang *et al*., "A Survey of Positioning Systems Using Visible LED Lights," in *IEEE Communications Surveys & Tutorials*, vol. 20, no. 3, pp. 1963-1988, thirdquarter 2018. doi: 10.1109/COMST.2018.2806558

[13] Sakpere, Wilson & Adeyeye Oshin, Michael & Mlitwa, Nhlanhla. (2017). A State-of-the-Art Survey of Indoor Positioning and Navigation Systems and Technologies. South African Computer Journal. 29. 145. 10.18489/sacj.v29i3.452.

[14] F. Zafari, A. Gkelias and K. K. Leung, "A Survey of Indoor Localization Systems and Technologies," in *IEEE Communications Surveys & Tutorials*, vol. 21, no. 3, pp. 2568-2599, thirdquarter 2019. doi: 10.1109/COMST.2019.2911558

[15] A.M. Ramirez-Aguilera, J.M. Luna-Rivera, V. Guerra, J. Rabadan, R. Perez-Jimenez, F.J. Lopez-Hernandez, “A review of indoor channel modeling techniques for visible light communication”, IEEE 10th Latin-American Conference on Communications (LATINCOM), 2018

[16] H. Q. Nguyen et al., "A MATLAB-based simulation program for indoor visible light communication system," 2010 7th International Symposium on Communication Systems, Networks & Digital Signal Processing (CSNDSP 2010), Newcastle upon Tyne, 2010, pp. 537-541, doi: 10.1109/CSNDSP16145.2010.5580355.

[17] Ramirez-Aguilera, Atziry & Luna-Rivera, J.M. & Yánez, Víctor & Rabadan, J. & Pérez-JIménez, Rafael & Hernández, Francisco. (2018). A generalized multi-wavelength propagation model for VLC indoor channels using Monte Carlo simulation. Transactions on Emerging Telecommunications Technologies. 30. e3490. 10.1002/ett.3490.

[18] F. R. Gfeller and U. Bapst, "Wireless in-house data communication via diffuse infrared radiation," in Proceedings of the IEEE, vol. 67, no. 11, pp. 1474-1486, Nov. 1979, doi: 10.1109/PROC.1979.11508.

[19] J. R. Barry, J. M. Kahn, W. J. Krause, E. A. Lee and D. G. Messerschmitt, "Simulation of multipath impulse response for indoor wireless optical channels," in IEEE Journal on Selected Areas in Communications, vol. 11, no. 3, pp. 367-379, April 1993, doi: 10.1109/49.219552.

[20] Lopez-Hernandez FJ, Perez-Jimenez R, SantamariaA.Monte Carlo calculation of impulse response on diffuse IR wireless indoor channels.
Electron Lett. 1998;34(12):1260-1262.

[21] J. Lopez-Hernandez, R. Perez-Jimenez and A. Santamaria, "Modified Monte Carlo scheme for high-efficiency simulation of the impulse response on diffuse IR wireless indoor channels," in Electronics Letters, vol. 34, no. 19, pp. 1819-1820, 17 Sept. 1998, doi: 10.1049/el:19981173.

[22] M. I. S. Chowdhury, W. Zhang and M. Kavehrad, "Combined Deterministic and Modified Monte Carlo Method for Calculating Impulse Responses of Indoor Optical Wireless Channels," in Journal of Lightwave Technology, vol. 32, no. 18, pp. 3132-3148, 15 Sept.15, 2014, doi: 10.1109/JLT.2014.2339131.

[23] Ramirez-Aguilera, AM, Luna-Rivera, JM, Guerra, V, Rabadan, J, Perez-Jimenez, R, Lopez-Hernandez, FJ. A generalized multi-wavelength propagation model for VLC indoor channels using Monte Carlo simulation. *Trans Emerging Tel Tech*. 2019; 30:e3490. https://doi.org/10.1002/ett.3490

[24] R. Perez-Jimenez, J. Berges and M. J. Betancor, "Statistical model for the impulse response on infrared indoor diffuse channels," in Electronics Letters, vol. 33, no. 15, pp. 1298-1300, 17 July 1997, doi: 10.1049/el:19970866.

[25] Santamaria, A., and Lopez-Hernandez. F J: “Wireless LAN Systems”, Artech-House, 1993

[26] Sarbazi E, Uysal M, Abdallah M, Qaraqe K. Indoor channel modelling and characterization for visible light communications. Paper presented at: 2014 16th International Conference on Transparent Optical Networks (ICTON); 2014; Graz, Austria.

[27] F. Miramirkhani and M. Uysal, "Channel Modeling and Characterization for Visible Light Communications," in IEEE Photonics Journal, vol. 7, no. 6, pp. 1-16, Dec. 2015, Art no. 7905616, doi: 10.1109/JPHOT.2015.2504238.

[28] H. Q. Nguyen et al., “A MATLAB-Based simulation program for indoor visible light communication system,” in Proc. CSNDSP, Jul. 2010, pp. 537–540.

[29] S. Long, M. A. Khalighi, M. Wolf, S. Bourennane, and Z. Ghassemlooy, “Channel characterization for indoor visible light communications,” in Proc. IWOW, Sep. 2014, pp. 75–79.

[30] Demtröder, Wolfgang (2012): Experimentalphysik 2. Heidelberg: Springer Spektrum. Page 262

[31] J. Wang, A. Al-Kinani, W. Zhang and C. Wang, "A new VLC channel model for underground mining environments," 2017 13th International Wireless Communications and Mobile Computing Conference (IWCMC), pp. 2134-2139, 2017

[32] Y. Zhuang *et al*., "A Survey of Positioning Systems Using Visible LED Lights," in *IEEE Communications Surveys & Tutorials*, vol. 20, no. 3, pp. 1963-1988, thirdquarter 2018. doi: 10.1109/COMST.2018.2806558

[33] T. Wenge, M. T. Chew, F. Alam and G. S. Gupta, "Implementation of a visible light based indoor localization system," *2018 IEEE Sensors Applications Symposium (SAS)*, Seoul, 2018, pp. 1-6. doi: 10.1109/SAS.2018.8336711

[34] Bergen, M.H.; Schaal, F.S.; Klukas, R.; Cheng, J.; Holzman, J.F. Toward the implementation of a universal
angle-based optical indoor positioning system. Front. Optoelectron. 2018, 11, 116–127.

[35] Zhu, B.; Cheng, J.; Wang, Y.; Yan, J.; Wang, J. Three-Dimensional VLC Positioning Based on Angle Difference
of Arrival with Arbitrary Tilting Angle of Receiver. IEEE J. Sel. Areas Commun. 2018, 36, 8–22.

[36] Kuo, Y.-S.; Pannuto, P.; Hsiao, K.-J.; Dutta, P. Luxapose: Indoor positioning with mobile phones and visible
light. In Proceedings of the Annual International Conference on Mobile Computing and Networking, MOBICOM, Maui, HI, USA, 7–11 September 2014; pp. 447–458.

[37] C. He, S. Cincotta, M. M. A. Mohammed and J. Armstrong, "Angular Diversity Aperture (ADA) Receivers for Indoor Multiple-Input Multiple-Output (MIMO) Visible Light Communications (VLC)," in *IEEE Access*, vol. 7, pp. 145282-145301, 2019. doi: 10.1109/ACCESS.2019.2945075

[38] P. Fahamuel, J. Thompson and H. Haas, "Improved indoor VLC MIMO channel capacity using mobile receiver with angular diversity detectors," *2014 IEEE Global Communications Conference*, Austin, TX, 2014, pp. 2060-2065. doi: 10.1109/GLOCOM.2014.7037111

[39] L. Wang and C. Guo, "Indoor Visible Light Localization Algorithm with Multi-Directional PD Array," 2017 IEEE Globecom Workshops (GC Wkshps), Singapore, 2017, pp. 1-6. doi: 10.1109/GLOCOMW.2017.8269149

[40] A. Nuwanpriya, S. Ho and C. S. Chen, "Indoor MIMO Visible Light Communications: Novel Angle Diversity Receivers for Mobile Users," in *IEEE Journal on Selected Areas in Communications*, vol. 33, no. 9, pp. 1780-1792, Sept. 2015. doi: 10.1109/JSAC.2015.2432514

[41] Z. Zeng, M. D. Soltani, M. Safari and H. Haas, "Angle Diversity Receiver in LiFi Cellular Networks," *ICC 2019 - 2019 IEEE International Conference on Communications (ICC)*, Shanghai, China, 2019, pp. 1-6. doi: 10.1109/ICC.2019.8761200

[42] L. Wei, H. Zhang, B. Yu, J. Song and Y. Guan, "Cubic-Receiver-Based Indoor Optical Wireless Location System," in *IEEE Photonics Journal*, vol. 8, no. 1, pp. 1-7, Feb. 2016, Art no. 7901207. doi: 10.1109/JPHOT.2016.2519281

[43] T. Q. Wang, Y. A. Sekercioglu and J. Armstrong, "Analysis of an Optical Wireless Receiver Using a Hemispherical Lens With Application in MIMO Visible Light Communications," in *Journal of Lightwave Technology*, vol. 31, no. 11, pp. 1744-1754, June1, 2013. doi: 10.1109/JLT.2013.2257685

[44] T. Q. Wang, R. J. Green and J. Armstrong, "Prism array-based receiver with application in MIMO indoor optical wireless communications," *2014 16th International Conference on Transparent Optical Networks (ICTON)*, Graz, 2014, pp. 1-4. doi: 10.1109/ICTON.2014.6876577

[45] T. Q. Wang, R. J. Green and J. Armstrong, "MIMO Optical Wireless Communications Using ACO-OFDM and a Prism-Array Receiver," in *IEEE Journal on Selected Areas in Communications*, vol. 33, no. 9, pp. 1959-1971, Sept. 2015. doi: 10.1109/JSAC.2015.2432520

[46] T. Q. Wang, C. He and J. Armstrong, "Performance Analysis of Aperture-Based Receivers for MIMO IM/DD Visible Light Communications," in *Journal of Lightwave Technology*, vol. 35, no. 9, pp. 1513-1523, 1 May1, 2017. doi: 10.1109/JLT.2016.2641002

[47] J. Song, L. Wei and H. Zhang, "Deflected field-of-views receiver for indoor MIMO visible light communications," *2017 International Conference on Infocom Technologies and Unmanned Systems (Trends and Future Directions) (ICTUS)*, Dubai, 2017, pp. 11-17. doi: 10.1109/ICTUS.2017.8285966

[48] H. Steendam, T. Q. Wang and J. Armstrong, "Cramer-Rao bound for indoor visible light positioning using an aperture-based angular-diversity receiver," *2016 IEEE International Conference on Communications (ICC)*, Kuala Lumpur, 2016, pp. 1-6. doi: 10.1109/ICC.2016.7510822

[49] H. Steendam, T. Q. Wang and J. Armstrong, "Theoretical Lower Bound for Indoor Visible Light Positioning Using Received Signal Strength Measurements and an Aperture-Based Receiver," in *Journal of Lightwave Technology*, vol. 35, no. 2, pp. 309-319, 15 Jan.15, 2017. doi: 10.1109/JLT.2016.2645603

[50] E. Aparicio-Esteve, Á. Hernández, J. Ureña, J. M. Villadangos and F. Ciudad, "Estimation of the Polar Angle in a 3D Infrared Indoor Positioning System based on a QADA receiver," *2019 International*

Conference on Indoor Positioning and Indoor Navigation (IPIN), Pisa, Italy, 2019, pp. 1-8. doi: 10.1109/IPIN.2019.8911775

[51] S. Cincotta, C. He, A. Neild, and J. Armstrong, "High angular resolution visible light positioning using a quadrant photodiode angular diversity aperture receiver (QADA)," Opt. Express 26, 9230-9242 (2018).

[52] S. Cincotta, C. He, A. Neild and J. Armstrong, "QADA-PLUS: A Novel Two-Stage Receiver for Visible Light Positioning," *2018 International Conference on Indoor Positioning and Indoor Navigation (IPIN)*, Nantes, 2018, pp. 1-5. doi: 10.1109/IPIN.2018.8533733

[53] Cincotta, S.; He, C.; Neild, A.; Armstrong, J. Indoor Visible Light Positioning: Overcoming the Practical Limitations of the Quadrant Angular Diversity Aperture Receiver (QADA) by Using the Two-Stage QADA-Plus Receiver. *Sensors* **2019**, *19*, 956

[54] R. T. Valadas and A. M. de Oliveira Duarte, "Sectored receivers for indoor wireless optical communication systems," *5th IEEE International Symposium on Personal, Indoor and Mobile Radio Communications, Wireless Networks - Catching the Mobile Future.*, The Hague, Netherlands, 1994, pp. 1090-1095 vol.4. doi: 10.1109/WNCMF.1994.529423

[55] Mendoza, Beatriz R et al. “Comparison of Three Non-Imaging Angle-Diversity Receivers as Input Sensors of Nodes for Indoor Infrared Wireless Sensor Networks: Theory and Simulation.” *Sensors (Basel, Switzerland)* vol. 16,7 1086. 14 Jul. 2016, doi:10.3390/s16071086

[56] F. Lichtenegger, C. Leiner, C. Sommer, A. P. Weiss, F. P. Wenzl, *Ray-tracing based channel modelling for the simulation of the performance of visible light communication in an indoor environment*, Proc. of the Second Balkan Junior Conference on Lighting, Balkan Light Junior, (2019) DOI: 10.1109/BLJ.2019.8883669

[57] C. R. A. T. Lomba, R. T. Valadas and A. M. de Oliveira Duarte, "Sectored receivers to combat the multipath dispersion of the indoor optical channel," *Proceedings of 6th International Symposium on Personal, Indoor and Mobile Radio Communications*, Toronto, Ontario, Canada, 1995, pp. 321-325 vol.1. doi: 10.1109/PIMRC.1995.476906

[58] Yasir, M., Ho, S.-W., & Vellambi, B. N. (2014). *Indoor Positioning System Using Visible Light and Accelerometer. Journal of Lightwave Technology, 32(19), 33*